This manuscript is a generally clear description of an extended ocean biogeochemical model in the GENIE EMIC. However, a number of equations are wrong, so I recom- mend correcting these, rerunning the model, updating the figures, and if needed the text and conclusions. While this amounts to major revisions, I am hopeful that a revised manuscript would be acceptable.

We would like to thank the reviewer for a very thoughtful and constructive review.

Major comments: Line 244: “Finally organic matter (D) is made up of K size classes of organic matter, each containing i_d organic nutrient element pools. (Note that strictly speaking, detrital organic matter is not explicitly resolved as a state variable in ECOGEM as we currently only resolve the production of organic matter, which is passed to BIOGEM and held there as a state variable. As a consequence, there is no grazing on detrital organic matter in the current configuration of EcoGENIE. We include a description of D and its relationships here for completeness and for convenience of notation.” This is in fact a really inconvenient notation, because it obscures what happens in the model. See Line 452 below.

Please see our response to the comment relating to lines 452-455.

Line 294: “The size of the quota increases with [. . .] the loss of carbon.” First, this statement is not true, because in Section 3.2.7 it is pointed out that grazing loss does not affect stoichiometry, which is the correct thing to do.

We have now removed the preferential loss of carbon (through respiration) in response to a comment below. As such, we have also removed this statement, which is no longer applies to the updated model.

Secondly, Ikeda et al. (2001, DOI 10.1007/s002270100608) show that the stoichiometry of respiration is undistinguishable from the stoichiometry of biomass as well. This incorrect representation would lead to quota that are sometimes in excess of Qmax, which would give unrealistic artefacts in the nutrient cycling and potentially a violation of mass balance, and should therefore be corrected.

We have removed the independent loss of carbon from the model, as it can indeed violate mass balance in some conditions.

Line 301: This incorrect equation also appears in Geider et al. (1998, Limnol. Oceanogr. 43:679), although it is given here without attribution. Please use the correct equation from Morel (1987, J. Phycol. 23:137) max = himax – (himax – lomax)*(Q- Qmin)/(Qmax-Qmin)

As is the case for all models, both the Geider and Morel formulations have their issues. It is misleading to refer to either one as “correct” or “incorrect”. The Morel model, for example predicts that Q=Qmax when μ=μmax. This prediction is clearly refuted for non-limiting nutrients by Elrifi & Turpin (1985, J. Phycol., 21, 592–602). For the sake of maintaining consistency with Ward et al. (2012), we have chosen to retain the Geider et al. (2007) formulation.

Line 303: The appearance of γFe in the denominator of this equation is incorrect. It would make Chl synthesis increase as cells run out of iron, when in fact Chl:C decreases at low iron (Sunda and Huntsman 1997, Nature 390:389). A photosynthesis model that reproduces this iron limitation effect is given in Buitenhuis and Geider (2010, Limnol. Oceanogr. 55:714)

Assuming the reviewer means equation 13, The appearance of γFe in the denominator does not imply that Chl synthesis increases as cells become Fe limited, because, when Fe is limiting, γFe also appears the numerator (via P_C and P^{sat}; Equations 9 and 11).

Section 3.2.6 uses several words that have physiological meanings (limitation term, half saturation, inhibition) in a section describing light attenuation. If these sentences in fact deal with α (it would help to rename this to αChl), then it should be moved to Section 3.4.3. If it deals with light attenuation, it should be made clear how kChl is derived.

We have rearranged the text accordingly.

Line 343 : "length scale of 20 m" Is this used to calculate kw or the average value of ktot?

BIOGEM doesn't represent Chl, so water attenuates light with a constant optical depth. We have modified the text to clarify this.

"*In both BIOGEM and ECOGEM, the incoming shortwave solar radiation intensity is taken from the climate component in cGEnIE and varies seasonally (Edwards and Marsh, 2005b; Marsh et al., 2011). However, ECOGEM uses a slightly more complex light attenuation scheme than BIOGEM, which simply calculates a mean solar (shortwave) irradiance averaged over the depth of the surface layer, assuming a clear-water light attenuation scale of 20 m (Doney et al., 2006).*"

Line 345: "At the ocean surface" This would be a logical sentence to start the section.

We have rearranged the text to provide a more logical order to the sentence.

Between Line 452 and 455 D changes from 6 state variables in ECOGEM to 2 (C contents) in BIOGEM. Please explain what happens to the organic nutrient concentrations.

The ambiguity probably arose through our use of the singular in reference to the POM and DOM state-variable/flux vectors (each corresponding to three ECOGEM state-variables). We have changed the text to make it clear that there are 3 DOM state-variables and three POM fluxes in BIOGEM.

"*The dissolved organic matter vector (D1) includes three explicit tracers that are transported by the ocean circulation model and are degraded back to their constituent nutrients with a fixed turnover time of λ (= 0.5 years). Particulate organic matter (POM) is not represented with explicit state vari- ables in either ECOGEM or BIOGEM. Instead, its implicit production in the surface layer (and the corresponding export below the surface layer) is given by…*"

Line 533: It would make more sense to change e.g. the range between Qmin and Qmax, the partitioning between POM and DOM and the decay of POM with depth, which have much more uncertainty than the unrealistic choice noted in Line 294.

We have increased QminP (i.e. decreased max biomass C:P ratio) to compensate for the removal of C respiration.

Section 3.2.9: See comment on Line 294.

We have addressed the choice at line 294 above.

Figure 5 and Line 595: It is confusing to speak of POC production when there is no state variable for POC, and it leads to confusion with primary production. It would be easier to understand to speak of POC flux. Given the central importance of POC flux for air-sea CO2 flux and nutrient distributions, I suggest comparing it to observations (Schlitzer (2004), J. of Oceanography 60:53-62, https://lred.uea.ac.uk/web/green-ocean/data) and including these in Figures 3 and 19.

We have changed the text to describe POC flux rather than production.

"*The relative proportions in which these elements and compounds are exported from the surface ocean are regulated by the stoichiometry of biological production. In cGEnIE (BIOGEM), carbon 595 and phosphorus production are rigidly coupled through a fixed ratio of 106:1, while POFe:POC and CaCO3:POC production ratios are regulated as a function of environmental conditions. In ecoGEnIE (ECOGEM), phosphorus, iron and carbon production are all decoupled through the flexible quota physiology, which depends on both environmental conditions, and the status of the food-web. Only CaCO3:POC production ratios are regulated via the same mechanism in the two models (although 600 we decreased the average CaCO3:POC ratio in ECOGEM to compensate for the elevated POC production relative to POP).*"

We prefer not to use the Schlitzer POC flux dataset. It is based on data assimilation exercise in the North Pacific, and it is not clear how well it extrapolates to the global scale. Indeed, global estimates for vertical POC are still highly uncertain and even contradictory (see for example the discrepancy between Henson et al. doi:10.1029/2011GL046735, 2011 and Marsay et al. 10.1073/pnas.1415311112 2015), so we would prefer not to use these data as a benchmark of model performance.

Line 605: Rather than change ECOGEM to reproduce an arbitrary result in BIOGEM, it would be much more helpful to compare the CaCO3 export to observations (Lee (2001) Limnol. Oceanogr. 46: 1287–1297) and adjust the model to reproduce that.

The BIOGEM result was not arbitrary. It was from a model systematically calibrated to global phosphate and alkalinity measurements. An important aspect of the work here is traceably distinguishing the performance of ECOGEM and BIOGEM, so it is important to consistently evaluate the former against the latter.

Line 617: "total oceanic DIC inventory increased by just under 2% from 0.299 mol C" This makes no sense. The total oceanic DIC inventory is ~3.3 Examol.

Thanks for pointing this out. The 'Exa' prefix was omitted in error.

Line 652 and Figure 17: "The model predicts higher chlorophyll concentrations in the Southern Ocean" Figure 17 is inadequate to decide whether this is a reasonable comment to make.

This comment was in reference to Figure 14, which shows higher model chlorophyll concentrations in the Southern Ocean, relative to the SeaWiFS data.

Please have the y-axis range from 10-2 to 10 (values between 10-5 and 10-2 are insignificant), put the station names inside the panels, so that the panels can be made higher, and include the satellite chl in the figure.

The y-axis range was chosen to show the dynamic range of the model. Values < 1e-2 are indeed insignificant in the observations, but low winter values are an important component of the model dynamics. As such, we feel it is important to retain the y-axis range of 1e-5 to 1e1.

We have added SeaWiFs chlorophyll to the figure.

If that shows the in situ measurements span the satellite estimates, delete the Dierssen reference and rewrite this to reflect the findings of Le Quere et al. (2016, doi:10.5194/bg-13-4111-2016), that models underestimate SO chl because they underrepresent macrozooplankton. Also, after correcting the error on line 303, this may improve/decrease SO chl.

We have plotted SeaWiFS data at the three Southern Ocean sites. The satellite data do show a tendency to underestimate in situ observations on the Southern Ocean. We have therefore retained the Dierssen reference.

Figure 18 needs to be described.

We have added a description.

"*The seasonal cycles of primary production in the surface layer are compared to time-series observations in Figure 18. As also indicated in Figure 14, the spatial variance in modelled primary production is too low, with primary production overestimated at the most oligotrophic site (HOT) and typically underestimated at the most productive sites (esp. the equatorial Pacific, NABE and the Ross Sea). In contrast to the lack of spatial variability, the model exhibits significant seasonal variation, often in excess of the observed variability (at those sites where the seasonal cycle is well resolved).*"

Line 737: "the ecological community conforms to expectations in terms of standing stocks" This has not been shown. Comparison to Buitenhuis et al. (2013, doi:10.5194/essd-5-227-2013) would test this statement. Given the different definition of plankton groups, comparison could be made to Fig. 5a.

We have corrected this statement to read "*the ecological community conforms to expectations in terms of standing stocks and fluxes, both in terms of large-scale spatial distributions, and the seasonal cycles at specific locations (Figures 14 and 17)*".

Minor comments: Line 85: for the how -> for how Line 143: in terms its -> in terms of its Line 162: modularised -> modular Line 176: a greater intention to explore long timescale -> the intention to explore longer timescale Line 262: the the -> the Line 363: level the -> level of the Line 421: The O2:C ratio is in fact >1. Anderson and Sarmiento (1994) find it's ~170/117=1.45, so even 138/106 would be quite low, and it would be helpful to justify it. Line 439: used equations -> used in equations Line 592: in tropical -> in the tropical Line 636: Figures 12 and 13 we -> In Figures 12 and 13 we Line 687: Figure 18 -> Figure 17 Line 690: is probably too low -> is too low

We will correct all these errors in the resubmitted manuscript. Note that the O2:CO2 ratio was inverted in error. This has been corrected.

Ward et al. present a new, size-based, marine ecosystem module for the EMIC "GENIE", called "ECOGEM", that is intended to replace the simpler module "BIOGEM". They compare the results of two long-term simulations with these different ecosystem modules.

We would like to thank the reviewer for a very thoughtful and constructive review.

General Comments

The manuscript is generally well written; the ECOGEM equations are presented in a comprehensible way. Since this module has been used in a previous study (Ward et al. 2012), I will only comment on the specific use of ECOGEM in GENIE. Specifically, I am missing a critical discussion concerning ecosystem complexity versus simplifications in GENIE and possible problems related to light attenuation, export production (no prognostic variable for POC) and the neglect of physical transport of the ecosystem variables.

In addition, the results section must be improved as there are several shortcomings (see below); some figures are poorly explained.

Specific Comments

- title, line 158: please use a consistent terminology: either EcoGE**n**IE or EcoGE**N**IE

  We have changed to GEnIE and EcoGEnIE throughout.

- line 21: please rephrase: fisheries is not "life in the ocean"

  Changed to "*support almost all life in the ocean, including the fish stocks that provide essential nutrition to more than half the human population*".

- line 25: since the reference is the latest but not the most common or original work, please use at least **e.g.** Hülse et al., 2017

  Changed.

- Figure 1: a similar figure for cGENIE and not only EcoGENIE would be helpful to immediately see the differences in complexity

  The figure currently includes the BIOGEM module (cGEnIE & EcoGEnIE) and the ECOGEM module (EcoGEnIE only). This think this should be sufficient for understanding the relationship between the two models.

- sections 3.2.5 Photoacclimation/3.2.6 Light attenuation: Please explicitly state that "photoacclimation" will not be relevant in this current ESM setup. The light attenuation in "GENIE" is overly simplified by assuming an *average* irradiance for the entire surface mixed layer and zero below. The idea to introduce a variable C:Chl ratio is mainly to allow for the development of subsurface chlorophyll maxima that do not correspond to phytoplankton biomass (carbon) maxima. Since the model resolution is too coarse and mean light levels are assumed, the C:Chl- ratio will not vary with depth.

  The C:Chl ratio also varies horizontally, as a function of PAR and nutrient availability. We included it to make comparisons to satellite data more meaningful.

lines 406/407: In my experience a minimum concentration of 1 x10^{-6} mmol C m^{-3} is high and will affect the results significantly; the variability and signals (like extinction) that might become relevant on longer time scales will be smeared out. A smaller value should be used at least for future studies.

Thanks for pointing this out.

- section 3.3.3 Dissolved organic matter: please explicitly state that export production within and below the mixed layer is the same (otherwise the figure caption in Figure 5 is confusing).

  Changed to "*implicit production in the surface layer (and the corresponding export below the surface layer) is given by…"*.

- section 4.2 Observations: the references for all observations must be properly provided (e.g. WOA09 is not sufficient)

  We now cite references for the GLODAPv2 and WOA data used. We also acknowledge the source of the SeaWiFs Chl data in the acknowledgements.

- section 5 Results: the entire section is presented in a very sloppy way. A few more explanations about why differences occur between the results of both model configurations or between model and observations are necessary. Please also provide the units for *all* quantities in *all* figures!

  Units are now included for all figures. We also provide a more complete description of the results (e.g. description of Figure 18).

- section 5.1.1 Global surface values: there is general agreement that primary production in the Southern Ocean (the largest HNLC area) is limited by iron, which explains the high macronutrient (e.g. phosphate) concentrations. ESMs generally overestimate the iron concentrations and thus nutrient uptake in the SO. Although the phosphate concentrations in the SO (Fig. 3) are difficult to identify, it seems to me that this is the case here, too. Is it true?

  The high surface PO4 concentrations in the SO are likely a consequence of low Fe, low irradiance (deep mixing) and cold temperatures.

- line 683: please be more specific. The general statement "Iron limitation in high latitude regions" is wrong. As far as I can deduce from Figure 16, iron limitation occurs mainly in the Southern Ocean and the western part of the North Subarctic Pacific Ocean.

  Fe limitation is clearly seen in all high latitude regions (especially among the larger phytoplankton size classes). We have adjusted the text to highlight this in Figure 16.

  "*Iron limitation dominates in high latitude regions, especially among larger size classes. Among these larger groups, the upwelling zones appear to be characterised by iron-phosphorus co-limitation."*

- line 711: "costs" should be used here instead of "overheads".

  Changed.

- all Figures showing spatial maps: what does the number 10000 on the North American continent refer to?

  This was the model integration year. It has been removed from all figures.

Manuscript prepared for Geosci. Model Dev.
with version 2015/09/17 7.94 Copernicus papers of the LaTeX class copernicus.cls.
Date: 6 July 2018

EcoGEnIE ~~0.~~10.2: Plankton Ecology in the ~~cGENIE~~ cGEnIE Earth system model

Ben A. Ward[1,2,3], Jamie D. Wilson[1], Ros M. Death[1], Fanny M. Monteiro[1], Andrew Yool[2], and Andy Ridgwell[1,4]

[1]School of Geographical Sciences, University of Bristol, Bristol BS8 1SS, UK
[2]Ocean and Earth Science, University of Southampton, National Oceanography Centre, Southampton, UK
[3]National Oceanography Centre, Southampton, UK
[4]Department of Earth Sciences, University of California, Riverside CA, USA

Abstract. We present an extension to the ~~cGENIE~~ cGEnIE Earth System model that explicitly accounts for the growth and interaction of an arbitrary number of plankton species. The new package ('ECOGEM') replaces the implicit, flux-based, parameterisation of the plankton community currently employed, with explicitly resolved plankton populations and ecological dynamics. In ECOGEM, any number of plankton species, with ecophysiological traits (e.g. growth and grazing rates) assigned according to organism size and functional group (e.g. phytoplankton and zooplankton) can be incorporated at run-time. We illustrate the capability of the marine ecology enabled Earth system model ('~~EcoGENIE~~EcoGEnIE') by comparing results from one configuration of ECOGEM (with eight generic phytoplankton and zooplankton size classes) to climatological and seasonal observations. We find that the new ecological components of the model show reasonable agreement with both global-scale climatological and local-scale seasonal data. We also compare ~~EcoGENIE~~ EcoGEnIE results to a the existing biogeochemical incarnation of ~~cGENIE~~cGEnIE. We find that the resulting global-scale distributions of phosphate, iron, dissolved inorganic carbon, alkalinity and oxygen are similar for both iterations of the model. A slight deterioration in some fields in ~~EcoGENIE~~ EcoGEnIE (relative to the data) is observed, although we make no attempt to re-tune the overall marine cycling of carbon and nutrients here. The increased capabilities of ~~EcoGENIE~~ EcoGEnIE in this regard will enable future exploration of the ecological community on much longer timescales than have previously been examined in global ocean ecosystem models and particularly for past climates and global biogeochemical cycles.

1 Introduction

The marine ecosystem is an integral component of the Earth system and its dynamics. Photosynthetic plankton ultimately support almost all life in the ocean, including the ~~fisheries~~ fish stocks that provide essential nutrition to more than half the human population (Hollowed et al., 2013). In addition, the marine biota determine an important downward flux of carbon, known as the 'biological pump'.

This flux arises as biomass generated by photosynthesis in the well-lit ocean surface sinks into the dark ocean interior, where it is remineralised (~~Hülse et al., 2017~~)(e.g. Hülse et al., 2017). Modulated by the activity and composition of marine ecosystems, the biological pump increases the partial pressure of CO_2 at depth and decreases it in the ocean surface and atmosphere, and thus plays a key role in the regulation of Earth's climate. For instance, the existence of the biological carbon pump has been estimated to be responsible for an approximately 200 ppm decrease in atmospheric carbon concentration at steady state (Parekh et al., 2006), with variations in its magnitude being cited as playing a key role in, for example, the late Quaternary glacial-interglacial climate oscillations (Watson et al., 2000; Hain et al., 2014).

A variety of different marine biogeochemical modelling approaches have been developed in an attempt to understand how the marine carbon cycle functions and its dynamical interaction with climate, and to make both past and future projections. In the simplest of these approaches, the biological pump is incorporated into an ocean circulation (or box) model without explicitly including any state-variables for the biota. Such models have been described as models of 'biogenically induced chemical fluxes' (rather than explicitly of the biology - and ecology - itself; Maier-Reimer, 1993). They vary considerably in complexity, but can be broadly divided into two categories. In the first of these – 'nutrient-restoring' – models calculate the biological uptake of nutrients at any one point at the ocean surface as the flux required to maintain surface nutrient concentrations at observed values (e.g. Bacastow and Maier-Reimer, 1990; Najjar et al., 1992). The vertical flux is then remineralised at depth according to some attenuating profile, such as that of Martin et al. (1987). Within this framework, carbon export is typically calculated from the nutrient flux according to a fixed stoichiometric ('Redfield') ratio (Redfield, 1934). In addition to the availability of a spatially explicit (in the case of ocean circulation models) observed surface ocean nutrient field, nutrient restoring models inherently only require a single parameter – the restoring time-scale, and even this parameter is not critical (as long as the time-scale is sufficiently short that the model closely reproduces the observed nutrient concentrations). The simplicity of this approach lends itself to being able to focus on a very specific part of the ecosystem dynamics, namely the downward transport of organic matter, and was highly influential particularly during the early days of marine biogeochemical model development and assessment of carbon uptake and transport dynamics (e.g. Marchal et al., 1998; Najjar et al., 1992). However, because this approach is based explicitly upon observed values (or modified observations), they are primarily only suitable for diagnostic and modern steady-state applications and are unable to model any deviations of nutrient cycling, and hence of climate, from the current ocean state.

More sophisticated models of biogenically induced chemical fluxes do away with a direct observational constraint and instead estimate the organic matter export term on the basis of limiting factors, such as temperature, light and the availability of nutrients such as nitrogen, phosphorous and iron – an approach we will here refer to as 'nutrient-limitation'. Models based on this approach

(e.g. Bacastow and Maier-Reimer, 1990; Heinze et al., 1991; Archer and Johnson, 2000) were natural successors to the early nutrient restoring models and could account for the influence of multiple limiting nutrients and even implicitly partition export between different functional types (Watson et al., 2000). Without entraining an explicit dependence on observed surface ocean nutrient distributions, these models also now gain much more freedom and with it, a degree of predictive capability. Additionally, other than plausible values for nutrient half-saturation constants, nutrient-limitation models make few assumptions that are specifically tied to modern observations, and assume very little (if anything) about the particular organisms present. Hence, as long as one makes the assumption that the marine plankton that existed at some specific time in the past were physiologically similar, particularly in terms of fundamental nutrient requirements, there is no apparent reason why nutrient-limitation models will not be as applicable to much of the Phanerozoic in terms of geological past, as they are to the present (questions of how suitable they might be to the present in the first place, aside). Using nutrient-limitation flux schemes, marine biogeochemical cycles have hence already been simulated for periods such as the mid Cretaceous (Monteiro et al., 2012) and end Permian (Meyer et al., 2008), times for which surface nutrient distributions are not known *a priori*.

The disadvantage of both variants of models of biogenically induced chemical fluxes, is that they are not able to represent interactions between parts of the ecosystem (e.g. resource competition and predator-prey interactions), simply because these components and processes are not resolved. Nor can they address questions involving the addition or loss, such as associated with past extinction events, of plankton species and changes in ecosystem complexity and/or structure. They also suffer from being overly responsive to changes in nutrient availability. In the case of restoring models this is simply because any change in the target field will be closely tracked. In the case of the nutrient-limitation models, the lack of an explicit biomass term results in export fluxes changing instantaneously in response to changing limiting factors. In the real world, by contrast, sufficient biomass must first exist, such as in a bloom condition, in order to achieve maximal export. This has consequences for ~~the~~ how the seasonality of organic matter export is represented. Other restrictions include the inability to know anything about ecosystem size structure (and, by association, about particle sinking speed), or the degree of recycling at the ocean surface and hence the partitioning of carbon into dissolved vs. particulate phases in exported organic matter.

To allow models to respond to changes in ecosystem structure, and to incorporate some of the additional feedbacks and complexities that may be important in determining the future marine response to continued greenhouse gas emissions (Le Quéré et al., 2005), it has been necessary to explicitly resolve the ecosystem itself. Such models have been developed across a wide range of complexities (Kwiatkowski et al., 2014). Among the simplest are 'NPZD' type models, resolving a single nutrient, homogenous phytoplankton and zooplankton communities, and a single detrital pool (Wroblewski et al., 1988; Oschlies, 2001). At the other end of the spectrum, more complex models may include multiple nutrients and several 'Plankton Functional Types' (PFTs) (e.g. Aumont et al., 2003; Moore

et al., 2002; Le Quéré et al., 2005). What links these models is that the living state variables are very broadly based on ecological guilds (i.e. groups of organisms that exploit similar resources).

While simple NPZD models are capable of reproducing some of the observed variability in bulk properties such as chlorophyll biomass and primary production (Schartau and Oschlies, 2003b; Yool et al., 2013; Ward et al., 2013), their very simplicity precludes the representation of many potentially important biogeochemical processes and climate feedbacks. Additionally, NPZD models are parameterised to represent the activity of diverse plankton communities, with different parameter values being required as the ecosystem changes in space and time (Schartau and Oschlies, 2003a; Losa et al., 2006). In this regard, PFT models may be more generally applicable because they resolve relatively more fundamental ecological processes that may be less sensitive to environmental variability (Friedrichs et al., 2007). These are the key factors that have motivated the development of more complex models, in which the broad ecological guilds of NPZD models are replaced with more specific groups based on ecological and/or biogeochemical function (Aumont et al., 2015; Butenschön et al., 2016). It is argued that resolving more components of the ecosystem allows the representation of important climate feedbacks that cannot be accounted for in simpler models (Le Quéré, 2006).

However, alongside their advantages, the current generation of PFT models are faced with two important and conflicting challenges. Firstly, these complex models contain a large number of parameters that are often poorly constrained by observations (Anderson, 2005). Secondly, although PFT models resolve more ecological structure than the preceding generation of ocean ecosystem models, they are rarely general enough to perform well across large environmental gradients (Friedrichs et al., 2006, 2007; Ward et al., 2010). To these, one might add difficulties in their application to past climates. PFT models are based on a conceptual reduction of the modern marine ecosystem to its apparent key biogeochemical components, such as nitrogen fixation, or opal frustule production (as by diatoms). The role of diatoms and the attendant cycling of silica quickly becomes moot once one looks back in Earth history as the origin of diatoms is thought to be sometime early in the Mesozoic (252-66 Ma) and they did not proliferate and diversify until later in the Cenozoic (66-0 Ma) (Falkowski et al., 2004). In addition, the physiological details of each species encoded in the model are taken directly from laboratory culture experiments of isolated strains (Le Quéré et al., 2005) creating a parameter-dependence on modern cultured species, in addition to a structural one.

Recent studies have begun to address these issues by focussing on the more general rules that govern diversity (rather than by trying to quantify and parameterise the diversity itself). These 'trait-based' models are beginning to be applied in the field of marine biogeochemical modelling (e.g. Follows et al., 2007; Bruggeman and Kooijman, 2007), with a major advantage being that they are able to resolve greater diversity with fewer specified parameters. One of the main challenges of this approach then is to identify the general rules or trade-offs that govern competition between organisms (Follows et al., 2007; Litchman et al., 2007). These trade-offs are often strongly constrained by organism size. A potentially large number of different plankton size classes can therefore be pa-

rameterised according to well known allometric relationships linking plankton physiological traits to organism size (e.g. Tang, 1995; Hansen et al., 1997). This approach has the associated advantage that the size composition of the plankton community affects the biogeochemical function of the community (e.g. Guidi et al., 2009). If one assumes that the same allometric relationships and trade-offs are relatively invariant with time, then this approach provides a potential way forward to addressing geological questions.

In this paper we present an adaptable modelling framework with an ecological structure that can be easily adapted according to the scientific question at hand. The model is formulated so that all plankton are described by the same set of equations, and any differences are simply a matter of parameterisation. Within this framework, each plankton population is characterised in terms of its size-dependent traits and its distinct functional type. The model also includes a realistic physiological component, based on a cell quota model (Caperon, 1968; Droop, 1968) and a dynamic photoacclimation model (Geider et al., 1998). This physiological component increases model realism by allowing phytoplankton to flexibly take up nutrients according to availability, rather than according to an unrealistically rigid cellular stoichiometry. Such flexible stoichiometry is rarely included in large-scale ocean models, and provides the opportunity to study the links between plankton physiology, ecological competition, and biogeochemistry. This model is then embedded within an Earth system model (~~eGENIE~~cGEnIE) widely used in addressing questions of past climate and carbon cycling, and the overall properties of the model system are evaluated.

The structure of this paper is as follows. In Section ~~??~~ 2 we will briefly outline the nature and properties of the ~~eGENIE~~ cGEnIE Earth system model, focussing on the ocean circulation and marine biogeochemical modules most directly relevant to the simulation of marine ecology. In Section 3, we introduce the new ecological model – ECOGEM – that has been developed within the ~~eGENIE~~ cGEnIE framework. Section 4 describes the preliminary experiments of ECOGEM, and Section 5 presents results from the new integrated global model (EcoGEnIE) in comparison to observations (where available) as well as to the pre-existing biogeochemical simulation of ~~eGENIE~~cGEnIE.

2 The ~~GENIE~~GEnIE/~~eGENIE~~ cGEnIE Earth system model

~~GENIE~~ GEnIE is an 'Earth system model of intermediate complexity' (EMIC) (Claussen et al., 2002) and is based on a ~~modularised~~ modular framework that allows different components of the Earth system, including ocean circulation, ocean biogeochemistry, deep-sea sediments and geochemistry, to be incorporated (Lenton et al., 2007). The simplified atmosphere and carbon-centric version of ~~GENIE~~ GEnIE we use – ~~eGENIE~~cGEnIE – has been previously applied to explore and understand the interactions between biological productivity, biogeochemistry and climate over a range of timescales and time periods (e.g., Ridgwell and Schmidt, 2010; Monteiro et al., 2012; Norris et al., 2013; John et al., 2014; Gibbs et al., 2015; Meyer et al., 2016; Tagliabue et al., 2016). As is

common for EMICs, ~~eGENIE~~ cGEnIE features a decreased spatial and temporal resolution in order to facilitate the efficient simulation of the various interacting components. This imposes limits on the resolution of ecosystem dynamics to large-scale annual/seasonal patterns in contrast to higher resolutions often used to model modern ecosystems. However, our motivation for incorporating a new marine ecosystem module into ~~eGENIE~~ cGEnIE is to focus on the explicit interactions between ecosystems, biogeochemistry and climate that are computationally prohibitive in higher resolution models. In other words, our motivation is to include and explore a more complete range of interactions and dynamics within the marine system, at the expense of spatial fidelity and with ~~a greater~~ the intention to explore long timescale and paleoceanographic questions, rather than short-term and future anthropogenic concerns.

2.1 Ocean physics and climate model component – C-GOLDSTEIN

The fast climate model, C-GOLDSTEIN features a reduced physics (frictional geostrophic) 3-D ocean circulation model coupled to a 2-D energy-moisture balance model of the atmosphere and a dynamic-thermodynamic sea-ice model. Full descriptions of the model can be found in Edwards and Marsh (2005a) and Marsh et al. (2011).

The circulation model calculates the horizontal and vertical transport of heat, salinity, and biogeochemical tracers via the combined parameterisation for isoneutral diffusion and eddy-induced advection (Edwards and Marsh, 2005a; Marsh et al., 2011). The ocean model is configured on a 36×36 equal-area horizontal grid with 16 logarithmically spaced z-coordinate levels. The horizontal grid is generally constructed to be uniform in longitude (10° resolution) and uniform in the sine of latitude (varying in latitude from ~3.2° at the equator to 19.2° near the poles). The thickness of the vertical grid increases with depth, from 80.8 m at the surface, to as much as 765 m at depth. The degree of spatial and temporal abstraction in C-GOLDSTEIN results in parameter values that are not well known and require calibration against observations. The parameters for C-GOLDSTEIN were calibrated against annual mean climatological observations of temperature, salinity, surface air temperature and humidity using the ensemble Kalman filer (EnKF) methdology (Hargreaves et al., 2004; Ridgwell et al., 2007a). The parameter values for C-GOLDSTEIN used are those reported for the 16-level model in Table S1 of Cao et al. (2009) under "~~GENIE16~~GEnIE16". C-GOLDSTEIN is run with 96 time-steps per year. The resulting circulation is dynamically similar to that of classical GCMs based on the primitive equations but is significantly faster to run and in this configuration performs well against standard tests of circulation models such as anthropogenic CO_2 and CFC uptake, as well as reproducing the deep ocean radiocarbon ($\Delta^{14}C$) distribution (Cao et al., 2009).

2.2 Ocean biogeochemical model component – BIOGEM

Transformations and spatial redistribution of biogeochemical compounds both at the ocean surface (by biological uptake) and in the ocean interior (remineralisation), plus air-sea gas exchange, are han-

dled by the module BIOGEM. In the pre-existing version of BIOGEM the biological (soft-tissue) pump is driven by an implicit (i.e. unresolved) biological community (in place of an explicit representation of living microbial community). It is therefore a nutrient limitation variant of a model of biogenically induced chemical fluxes, as outlined above. A full description can be found in (Ridgwell et al., 2007a; Ridgwell and Death, in prep.).

In this study, we use a seasonally insolation forced, 16-level ocean model configuration, similar to that of Cao et al. (2009). However, in the particular biogeochemical configuration we use, limitation of biological uptake of carbon is provided by the availability of two nutrients. In addition to phosphate, we now include an iron cycle following (Tagliabue et al., 2016). This aspect of the model is determined by a revised set of parameters controlling the iron cycle (Ridgwell and Death, in prep.). We also incorporate a series of minor modifications to the climate model component, particularly in terms of the ocean grid and wind velocity and stress forcings (consistent with Marsh et al., 2011) together with associated changes to several of the physics parameters. A complete description and evaluation of the physical and biogeochemical configuration of ~~cGENIE~~ cGEnIE is provided in (Ridgwell and Death, in prep.).

3 Ecological model component – ECOGEM

The current BIOGEM module in ~~cGENIE~~ cGEnIE does not explicitly resolve the biological community and instead transforms surface inorganic nutrients directly into export:

- inorganic nutrients $\xrightarrow[\text{and export}]{\text{production}}$ DOM and remineralised nutrients

This simplification greatly facilitates the efficient modelling of the carbon cycle over long time scales, but with the associated caveats of an implicit scheme (as discussed earlier). In ECOGEM, biological uptake is again limited by light, temperature and nutrient availability, but here it must pass through an explicit and dynamic intermediary plankton community, before being returned to DOM or dissolved inorganic nutrients:

- inorganic nutrients $\xrightarrow{\text{production}}$ living biomass $\xrightarrow{\text{export}}$ DOM and remineralised nutrients

The ecological community is also subject to ~~respiration,~~ mortality and internal trophic interactions, and will produce both inorganic compounds and organic matter. The structural relationship between BIOGEM and ECOGEM is illustrated in Figure 1.

In the following section we outline the key state variables directly relating to ecosystem function (Section 3.1), describe the mathematical form of the key rate processes relating to each state variable (Section 3.2) and how they link together (Section 3.3). We will then describe the parameterisation of the model according to organism size and functional type (Section 3.4). The model equations are modified from Ward et al. (2012). We provide all the equations used in ECOGEM here, but we

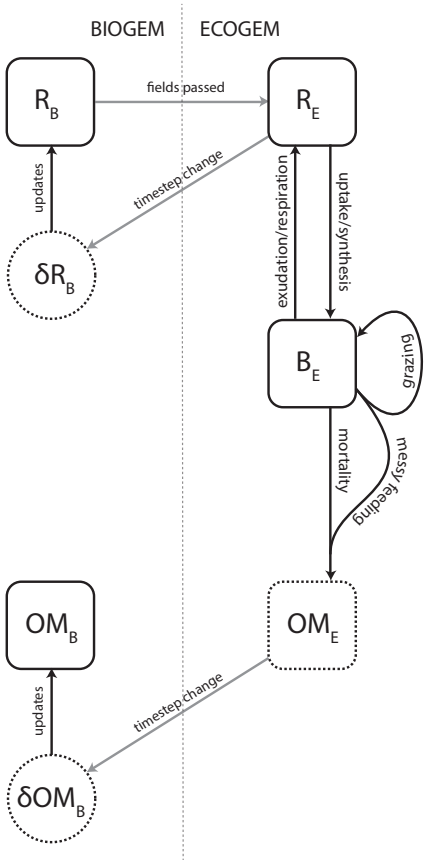

Figure 1. Schematic representation of the coupling between BIOGEM and ECOGEM. State variables: R = inorganic element (i.e. resource), B = plankton biomass, OM = organic matter. Subsripts $_B$ and $_E$ denote state variables in BIOGEM and ECOGEM, respectively. BIOGEM passes resource biomass R to ECOGEM. ECOGEM passes rates of change (δ) in R and OM back to BIOGEM.

provide only brief descriptions of the parameterisations and parameter value justifications already included in Ward et al. (2012).

3.1 State variables

ECOGEM state variables are organised into three matrices (Table 1), representing ecologically-relevant biogeochemical tracers (hereafter referred to as 'nutrient resources'), plankton biomass and organic matter. All these matrices have units of mmol element m^{-3}, with the exception of the dynamic chlorophyll quota, which is expressed in units of mg chlorophyll m^{-3}. The nutrient resource matrix ($\mathbf{R}$) includes I_r distinct inorganic resources. The plankton community ($\mathbf{B}$) is made up of J individual populations, each associated with I_b cellular nutrient quotas. Finally organic matter ($\mathbf{D}$) is made up of K size classes of organic matter, each containing i_d organic nutrient element pools. (Note that strictly speaking, detrital organic matter is not explicitly resolved as a state variable in

ECOGEM as we currently only resolve the production of organic matter, which is passed to BIOGEM and held there as a state variable. As a consequence, there is no grazing on detrital organic matter in the current configuration of ~~EcoGENIE~~EcoGEnIE. We include a description of $\mathbf{D}$ and its relationships here for completeness and for convenience of notation.)

Table 1. State variable index notation.

State variable	Dimensions	Index	Size	Available elements
$\mathbf{R}$	Resource element	i_r	I_r	DIC, PO_4, Fe
$\mathbf{B}$	Plankton class	j	J	1, 2, ..., J
	Cellular quota	i_b	I_b	C, P, Fe, Chl
$\mathbf{D}$	Organic matter size class	k	K	DOM, POM
	Detrital nutrient element	i_d	I_d	C, P, Fe

3.1.1 Inorganic resources

$\mathbf{R}$ is a row vector of length I_r, the number of dissolved inorganic nutrient resources.

$$\mathbf{R} = \begin{bmatrix} DIC & PO_4 & Fe \end{bmatrix} \tag{1}$$

An individual inorganic resource is denoted by the appropriate subscript. For example, PO_4 is denoted R_{PO_4}.

3.1.2 Plankton biomass

$\mathbf{B}$ is a $J \times I_b$ matrix, where J is the number of plankton populations and I_b is the number of cellular quotas, including chlorophyll.

$$\mathbf{B} = \begin{bmatrix} B_{1,C} & B_{1,P} & B_{1,Fe} & B_{1,Chl} \\ B_{2,C} & B_{2,P} & B_{2,Fe} & B_{2,Chl} \\ \vdots & \vdots & \vdots & \vdots \\ B_{J,C} & B_{J,P} & B_{J,Fe} & B_{J,Chl} \end{bmatrix} \tag{2}$$

Each population and element is denoted by an appropriate subscript. For example, the total carbon biomass of plankton population j is denoted $B_{j,C}$, while the chlorophyll biomass of that population is denoted $B_{j,Chl}$. The column vector describing the ~~the~~ carbon content of all plankton populations is denoted $\mathbf{B}_C$.

This framework can account for competition between (in theory) any number of different plankton populations. The model equations (below) are written in terms of an 'ideal' planktonic form, with the potential to exhibit the full range of ecophysiological traits (among those that are included in the model). Individual populations may take on a realistic subset of these traits, according to their

assigned 'plankton functional type' (PFT) (see Section 3.4.1). Each population is also assigned a characteristic size, in terms of equivalent spherical diameter (ESD) or cell volume. Organism size plays a key role in determining each population's ecophysiological traits (see Section 3.4.2).

3.1.3 Organic detritus

$\mathbf{D}$ is a $K \times I_d$ matrix, where K is the number of detrital size classes and I_d is the number of detrital nutrient elements.

$$\mathbf{D} = \begin{bmatrix} D_{1,C} & D_{1,P} & D_{1,Fe} \\ D_{2,C} & D_{2,P} & D_{2,Fe} \end{bmatrix} \tag{3}$$

Each size class and element is denoted by an appropriate subscript. For example, dissolved organic phosphorus (size class $k = 1$) is denoted $D_{1,P}$, while particulate organic iron (size class $k = 2$) is denoted $D_{2,Fe}$.

3.2 Plankton physiology and ecology

The rates of change in each state variable within ECOGEM are defined by a range of ecophysiological processes. These are defined by a set of mathematical functions that are common to all plankton populations. Parameter values are defined in Section 3.4.

3.2.1 Temperature limitation

Temperature affects a wide range of metabolic processes through an Arrenhius-like equation that is here set equal for all plankton.

$$\gamma_{\mathrm{T}} = e^{A(\mathrm{T} - T_{\mathrm{ref}})} \tag{4}$$

The parameter A describes the temperature sensitivity, T is the ambient water temperature in degrees C, and T_{ref} is a reference temperature (also in degrees C) at which $\gamma_{\mathrm{T}} = 1$.

3.2.2 The plankton 'quota'

The physiological status of a plankton population is defined in terms of its cellular nutrient quota, $\mathbf{Q}$, which is the ratio of assimilated nutrient (phosphorus or iron) to carbon biomass. For each plankton population, j, and each planktonic quota, i_b ($\neq C$),

$$Q_{j,i_b} = \frac{B_{j,i_b}}{B_{j,C}} \tag{5}$$

This equation is also used to describe the population chlorophyll content relative to carbon biomass. The size of the quota increases with nutrient uptake ~~, chlorophyll synthesis, or the loss of carbon~~or chlorophyll synthesis. The quota decreases through the acquisition of carbon (described below).

Excessive accumulation of P or Fe biomass in relation to carbon is prevented as the uptake or assimilation of each nutrient element is down-regulated as the respective quota becomes full. The generic form of the uptake regulation term for element i_b is given by a linear function of the nutrient status, modified by an additional shape-parameter ~~(h=0.1)~~ (h=0.1; Geider et al., 1998) that allows greater assimilation under low-to-moderate resource limitation.

$$Q^{\mathrm{stat}}_{j,i_b} = \left(\frac{Q^{\mathrm{max}}_{j,i_b} - Q_{j,i_b}}{Q^{\mathrm{max}}_{j,i_b} - Q^{\mathrm{min}}_{j,i_b}} \right)^h \tag{6}$$

3.2.3 Nutrient uptake

Phosphate and dissolved iron ($i_r = i_b =$ P or Fe) are taken up as functions of environmental availability ($[R_{i_r}]$), maximum uptake rate (V^{max}_{j,i_r}), the nutrient affinity (α_{j,i_r}), the quota satiation term, ($Q^{\mathrm{stat}}_{j,i_b}$) and temperature limitation (γ_{T}):

$$V_{j,i_r} = \frac{V^{\mathrm{max}}_{j,i_r} \alpha_{j,i_r} [\mathrm{R_{i_r}}]}{V^{\mathrm{max}}_{j,i_r} + \alpha_{j,i_r} [\mathrm{R_{i_r}}]} Q^{\mathrm{stat}}_{j,i_b} \cdot \gamma_{\mathrm{T}} \tag{7}$$

This equation is effectively equivalent to the Michaelis-Menten type response, but replaces the half-saturation constant with the more mechanistic nutrient affinity, α_{j,i_r}.

3.2.4 Photosynthesis

The photosynthesis model is modified from Geider et al. (1998) and Moore et al. (2002). Light-limitation is calculated as a Poisson function of local irradiance (I), modified by the iron-dependent initial slope of the P-I curve ($\alpha \cdot \gamma_{j,\mathrm{Fe}}$) and the chlorophyll-$a$-to-carbon ratio ($Q_{j,\mathrm{Chl}}$).

$$\gamma_{j,I} = \left[1 - \exp\left(\frac{-\alpha \cdot \gamma_{j,\mathrm{Fe}} \cdot Q_{j,\mathrm{Chl}} \cdot I}{P^{\mathrm{sat}}_{j,\mathrm{C}}} \right) \right] \tag{8}$$

Here $P^{\mathrm{sat}}_{j,\mathrm{C}}$ is maximum light-saturated growth rate, modified from an absolute maximum rate of $P^{max}_{j,\mathrm{C}}$, according to the current nutrient and temperature limitation terms.

$$P^{sat}_{j,\mathrm{C}} = P^{max}_{j,\mathrm{C}} \cdot \gamma_T \cdot \min\left[\gamma_{j,\mathrm{P}},\ \gamma_{j,\mathrm{Fe}} \right] \tag{9}$$

The nutrient-limitation term is given as a minimum function of the internal nutrient status (Droop, 1968; Caperon, 1968; Flynn, 2008), each defined by normalised hyperbolic functions for P and Fe ($i_b =$ P or Fe),

$$\gamma_{j,i_b} = \frac{1 - Q^{\mathrm{min}}_{j,i_b}/Q_{j,i_b}}{1 - Q^{\mathrm{min}}_{j,i_b}/Q^{\mathrm{max}}_{j,i_b}}, \tag{10}$$

The gross photosynthetic rate ($P_{j,\mathrm{C}}$) is then modified from $P^{sat}_{j,\mathrm{C}}$ by the light-limitation term.

$$P_{j,\mathrm{C}} = \gamma_{j,I} P^{\mathrm{sat}}_{j,\mathrm{C}} \tag{11}$$

Net carbon uptake is given by

$$V_{j,\mathrm{C}} = P_{j,\mathrm{C}} - \xi \cdot V_{j,\mathrm{P}} \tag{12}$$

With the second term accounting for the metabolic cost of biosynthesis (ξ). This parameter was originally defined as a loss of carbon as a fraction of nitrogen uptake (Geider et al., 1998). We define it here relative to phosphate uptake, using a fixed N:P ratio of 16.

3.2.5 Photoacclimation

The chlorophyll-to-carbon ratio is regulated as the cell attempts to balance the rate of light capture by chlorophyll with the maximum potential (i.e. light-replete) rate of carbon fixation. Depending on this ratio, a certain fraction of newly assimilated phosphorus is diverted to the synthesis of new chlorophyll a,

$$\rho_{j,\mathrm{Chl}} = \theta_{\mathrm{P}}^{\max} \frac{P_{j,\mathrm{C}}}{\alpha \cdot \gamma_{j,\mathrm{Fe}} \cdot Q_{j,\mathrm{Chl}} \cdot I} \tag{13}$$

Here $\rho_{j,\mathrm{Chl}}$ is the amount of chlorophyll a that is synthesised for every mmol of phosphorus assimilated (mg Chl (mmol P)$^{-1}$) with $\theta_{\mathrm{P}}^{\max}$ representing the maximum ratio (again converting from the nitrogen based units of Geider et al., 1998, with a fixed N:P ratio of 16). If phosphorus is assimilated at carbon specific rate $V_{j,\mathrm{P}}$ (mmol P (mmol C)$^{-1}$ d^{-1}), then the carbon specific rate of chlorophyll a synthesis (mg chl (mmol C)$^{-1}$ d^{-1}) is

$$V_{j,\mathrm{Chl}} = \rho_{j,\mathrm{Chl}} \cdot V_{j,\mathrm{P}} \tag{14}$$

3.2.6 Light attenuation

~~ECOGEM~~ In both BIOGEM and ECOGEM, the incoming shortwave solar radiation intensity is taken from the climate component in cGEnIE and varies seasonally (Edwards and Marsh, 2005b; Marsh et al., 2011). However, ECOGEM uses a slightly more complex light attenuation scheme than BIOGEM, which simply calculates a mean solar (shortwave) irradiance averaged over the depth of the surface layer, ~~and assuming a length~~ assuming a clear-water light attenuation scale of 20 m ~~over which light decays (Doney et al., 2006). BIOGEM then takes this mean irradiance and applies a Michaelis-Menten like limitation term, assuming a half saturation value for light of 20 W m^{-2} (Doney et al., 2006). At the ocean surface, the incoming shortwave solar radiation intensity is taken from the climate component in cGENIE and varies seasonally (Edwards and Marsh, 2005b; Marsh et al., 2011). (Doney et al., 2006)~~ .

In ECOGEM the light level is calculated as the mean level of photosynthetically available radiation within a variable mixed layer (with depth calculated according to Kraus and Turner, 1967). We also take into account inhibition of light penetration due to the presence of light absorbing particles and dissolved molecules (Shigsesada and Okubo, 1981). If Chl_{tot} is the total chlorophyll concentration in the surface layer (of thickness Z_1), and Z_{ML} is the mixed-layer depth, the virtual chlorophyll concentration distributed across the mixed layer is given by

$$Chl_{ML} = Chl_{tot} \frac{Z_1}{Z_{ML}} \tag{15}$$

The combined light-attenuation coefficient attributable to both water and the virtual chlorophyll concentration is given by

$$k_{tot} = k_w + k_{chl} \cdot Chl_{ML} \tag{16}$$

For a given level of photosynthetically available radiation at the ocean surface (I_0), plankton in the surface grid box experience the average irradiance within the mixed layer, which is given by

$$I = \frac{I_0}{k_{tot}} \frac{1}{Z_{ML}} (1 - e^{(-k_{tot} \cdot Z_{ML})}) \tag{17}$$

3.2.7 Predation (including both herbivorous and carnivorous interactions)

Here we define predation simply as the consumption of any living organism, regardless of the trophic level of the organism (i.e. phytoplankton or zooplankton prey).

The predator-biomass-specific grazing rate of predator (j_{pred}) on prey (j_{prey}) is given by,

$$G_{j_{\mathrm{pred}},j_{\mathrm{prey}},\mathrm{C}} = \gamma_{\mathrm{T}} \cdot \underbrace{G^{\max}_{j_{\mathrm{pred}},\mathrm{C}} \cdot \frac{\mathcal{F}_{j_{\mathrm{pred}},\mathrm{C}}}{k_{j_{prey},\mathrm{C}} + \mathcal{F}_{j_{\mathrm{pred}},\mathrm{C}}}}_{\text{overall grazing rate}} \cdot \underbrace{\Phi_{j_{\mathrm{pred}},j_{\mathrm{prey}}}}_{\text{switching}} \cdot \underbrace{(1 - e^{\Lambda \cdot \mathcal{F}_{j_{\mathrm{pred}},\mathrm{C}}})}_{\text{prey refuge}} \tag{18}$$

where γ_{T} is the temperature-dependence, $G^{\max}_{j_{\mathrm{pred}},\mathrm{C}}$ is the maximum grazing rate, and $k_{j_{prey},\mathrm{C}}$ is the half-saturation concentration for all (available) prey. The overall grazing rate is a function of total food available to the predator, $\mathcal{F}_{j_{\mathrm{pred}},\mathrm{C}}$. This is given by the product of the prey biomass vector, $\mathbf{B}_{\mathrm{C}}$, and the grazing kernel ($\boldsymbol{\phi}$),

$$\underset{[J_{\mathrm{pred}} \times 1]}{\boldsymbol{\mathcal{F}}_{\mathrm{C}}} = \underset{[J_{\mathrm{pred}} \times J_{\mathrm{prey}}]}{\boldsymbol{\phi}} \underset{[J_{\mathrm{prey}} \times 1]}{\boldsymbol{B}_{\mathrm{C}}} \tag{19}$$

Note that this equation is written out in matrix form, with the dimensions noted underneath each matrix. Each element of the grazing matrix $\boldsymbol{\phi}$ is an approximately log-normal function of the predator-to-prey length ratio, $\vartheta_{j_{\mathrm{pred}},j_{\mathrm{prey}}}$, with an optimum ratio of ϑ_{opt} and a geometric standard deviation $\sigma_{j_{\mathrm{pred}}}$.

$$\phi_{j_{\mathrm{pred}},j_{\mathrm{prey}}} = \exp\Big[- \Big(\ln\big(\frac{\vartheta_{j_{\mathrm{pred}},j_{\mathrm{prey}}}}{\vartheta_{\mathrm{opt}}}\big) \Big)^2 / \big(2\sigma^2_{j_{\mathrm{pred}}}\big) \Big] \tag{20}$$

We also include an optional 'prey-switching' term, such that predators may preferentially attack those prey that are relatively more available (i.e. active switching, $s = 2$). Alternatively they may attack prey in direct proportion to their availability (i.e. passive switching, $s = 1$). In the simulations below we assume active switching.

$$\Phi_{j_{\mathrm{pred}},j_{\mathrm{prey}}} = \frac{(\phi_{j_{\mathrm{pred}},j_{\mathrm{prey}}} \mathrm{B}_{j_{\mathrm{prey}},\mathrm{C}})^s}{\sum_{j_{\mathrm{prey}}=1}^{J} (\phi_{j_{\mathrm{pred}},j_{\mathrm{prey}}} \mathrm{B}_{j_{\mathrm{prey}},\mathrm{C}})^s} \tag{21}$$

Finally, a prey refuge function is incorporated, such that the overall grazing rate is decreased when the availability of all prey ($\mathcal{F}_{j_{\mathrm{pred}},\mathrm{C}}$) is low. The size of the prey refuge is dictated by the coefficient

Λ. The overall grazing response is calculated on the basis of prey carbon. Grazing losses of other prey elements are simply calculated from their stoichiometric ratio to prey carbon, with different elements assimilated according to the predator's nutritional requirements (see below).

$$G_{j_{\mathrm{pred}},j_{\mathrm{prey}},\mathrm{i_b}} = G_{j_{\mathrm{pred}},j_{\mathrm{prey}},\mathrm{C}} \frac{\mathrm{B}_{j_{\mathrm{prey}},i_b}}{\mathrm{B}_{j_{\mathrm{prey}},\mathrm{C}}} \tag{22}$$

3.2.8 Prey assimilation

Prey biomass is assimilated into predator biomass with an efficiency of $\lambda_{j_{\mathrm{pred}},i_b}$ ($i_b \neq$ Chl). This has a maximum value of $\lambda^{\max}$ that is modified according the the quota status of the predator. For elements i_b = P or Fe, prey biomass is assimilated as a function of the respective predator quota. If the quota is full, the element is not assimilated. If the quota is empty, the element is assimilated with maximum efficiency ($\lambda^{\max}$).

$$\lambda_{j_{\mathrm{pred}},i_b} = \lambda^{\max} Q^{\mathrm{stat}}_{j,i_b} \tag{23}$$

C assimilation is regulated according to the status of the most limiting nutrient element (P or Fe) modified by the same shape-parameter, h, that was applied in Equation 6.

$$Q^{\mathrm{lim}}_{j,i_b} = \left(\frac{Q_{j,i_b} - Q^{\min}_{j,i_b}}{Q^{\max}_{j,i_b} - Q^{\min}_{j,i_b}} \right)^h \tag{24}$$

If both nutrient quotas are full, C is assimilated at the maximum rate. If either are empty, C assimilation is down-regulated until sufficient quantities of the limiting element(s) are acquired.

$$\lambda_{j_{\mathrm{pred}},\mathrm{C}} = \lambda^{\max} \min\left(Q^{\mathrm{lim}}_{j,\mathrm{P}}, Q^{\mathrm{lim}}_{j,\mathrm{Fe}}\right) \tag{25}$$

3.2.9 ~~Respiration~~

~~A linear respiration rate is applied to degrade plankton carbon biomass into dissolved inorganic carbon. This is achieved through a J by I_r respiration matrix, $\mathbf{r}$, which is non-zero only for i_r = DIC.~~

3.2.9 Death

All living biomass is subject to a linear mortality rate of m_p. This rate is decreased at very low biomasses (population carbon biomass $\lesssim 1{\times}10{-}6$ mmol C m^{-3}) in order to maintain a viable population within every surface grid cell ("everything is everywhere, but the environment selects", Baas-Becking, 1934).

$$m_j = m_p(1 - e^{-10^{10} \cdot B_{j,C}}) \tag{26}$$

The low biomass at which a population attains 'immortality' is sufficiently small for that population to have a negligible impact on all other components of the ecosystem.

3.2.10 Calcium carbonate

The production and export of calcium carbonate ($CaCO_3$) by calcifying plankton in the surface ocean is scaled to the export of particulate organic carbon via a spatially-uniform value which is modified by a thermodynamically-based relationship with the calcite saturation state. The dissolution of $CaCO_3$ below the surface is treated in a similar way to that of particulate organic matter (equation 32), as described by Ridgwell et al. (2007a) with the parameter values controlling the export ratio between $CaCO_3$ and POC taken from Ridgwell et al. (2007b).

3.2.11 Oxygen

Oxygen production is coupled to photosynthetic carbon fixation via a fixed linear ratio, such that

$$V_{j,O_2} = -\frac{106}{138}\frac{138}{106} V_{j,\mathrm{DIC}} B_{j,\mathrm{C}} \tag{27}$$

The negative sign indicates that oxygen is produced as DIC is consumed. Oxygen consumption associated with the remineralisation of organic matter is unchanged relative to BIOGEM.

3.2.12 Alkalinity

Production of alkalinity is coupled to planktonic uptake of PO_4 via a fixed linear ratio, such that

$$V_{j,Alk} = -16 V_{j,\mathrm{PO_4}} \cdot B_{j,\mathrm{C}} \tag{28}$$

The negative sign indicates that alkalinity increases as PO_4 is consumed. This relationship accounts for alkalinity changes associated with N transformations (Zeebe and Wolf-Gladrow, 2001) that are not explicitly represented in the biogeochemical configurations of ~~eGENIE~~ cGEnIE that are applied here.

3.2.13 Production of organic matter

Plankton mortality and grazing are the only two sources of organic matter, with partitioning between non-sinking dissolved and sinking particulate phases determined by the parameter β_j. In this initial implementation of ECOGEM, for traceability, the assumptions are the same as made in the current version of BIOGEM (Ridgwell and Death, in prep.) which themselves follow the OCMIP2 ocean carbon cycle modelling intercomparison protocol described in Najjar et al. (2007). Specifically, β_j is set to a fixed fraction β for all size classes.

3.3 Differential equations

Differential equations for $\mathbf{R}$, $\mathbf{B}$ and $\mathbf{D}$ are written below. The dimensions of each matrix and vector used in equations 29 to 31 are given in Table 1. Note that while $\mathbf{R}$ and $\mathbf{OM}$ are transported by the physical component of ~~GENIE~~GEnIE, living biomass $\mathbf{B}$ is not currently subject to any physical

transport. The only communication between biological communities in adjacent grid cells is through the advection and diffusion of inorganic resources and non-living organic matter in BIOGEM. Note that some additional sources and sinks of $\mathbf{R}$, and all sinks of $\mathbf{D}$, are computed in BIOGEM.

3.3.1 Inorganic resources

For each inorganic resource, i_r,

$$\frac{\partial R_{i_r}}{\partial t} = \sum_{j=1}^{J} \underbrace{-V_{j,i_r} \cdot B_{j,\mathrm{C}}}_{\text{uptake}} \pm \text{respiration} \tag{29}$$

3.3.2 Plankton biomass

For each plankton class, j, and internal biomass quota, i_b,

$$\frac{\partial B_{j,i_b}}{\partial t} = + \underbrace{V_{j,i_b} \cdot B_{j,C}}_{\text{uptake}} - \underbrace{m_j \cdot B_{j,i_b}}_{\text{basal mortality}} - \text{respiration} + \underbrace{B_{j,\mathrm{C}} \cdot \lambda_{j,i_b} \sum_{j_{\mathrm{prey}}=1}^{J} G_{j,j_{\mathrm{prey}},i_b}}_{\text{grazing gains}} - \underbrace{\sum_{j_{\mathrm{pred}}=1}^{J} B_{j_{\mathrm{pred}},\mathrm{C}} \cdot G_{j_{\mathrm{pred}},j,i_b}}_{\text{grazing losses}} \tag{30}$$

3.3.3 Dissolved organic matter

For each detrital nutrient element, i_d, the rate of change of dissolved fraction of organic matter ($k = 1$) is described by

$$\frac{\partial \mathrm{D}_{1,i_d}}{\partial t} = \underbrace{\sum_{j=1}^{J} [\mathrm{B}_{j,i_d}] \beta_j m_j}_{\text{mortality}} + \underbrace{\sum_{j_{\mathrm{pred}}=1}^{J} [\mathrm{B}_{j_{\mathrm{pred}},\mathrm{C}}](1-\lambda_{j_{\mathrm{pred}},i_b}) \sum_{j_{\mathrm{prey}}=1}^{J} \beta_{j_{\mathrm{prey}}} G_{j_{\mathrm{pred}},j_{\mathrm{prey}},i_d}}_{\text{messy feeding}} \tag{31}$$

~~Dissolved organic matter~~ The dissolved organic matter vector ($\mathbf{D}_1$) ~~is an explicit tracer that is~~ includes three explicit tracers that are transported by the ocean circulation model and ~~is~~ are degraded back to ~~its~~ their constituent nutrients with a fixed turnover time of λ (= 0.5 years). Particulate organic matter (POM) is not represented ~~as an explicit state variable~~ with explicit state variables in either ECOGEM or BIOGEM. Instead, its implicit production in the surface layer (and the corresponding export below the surface layer) is given by

$$F_{\text{surface},i_d} = \underbrace{\sum_{j=1}^{J} [\mathrm{B}_{j,i_d}](1-\beta_j) m_j}_{\text{mortality}} + \underbrace{\sum_{j_{\mathrm{pred}}=1}^{J} [\mathrm{B}_{j_{\mathrm{pred}},\mathrm{C}}](1-\lambda_{j_{\mathrm{pred}},i_b}) \sum_{j_{\mathrm{prey}}=1}^{J} (1-\beta_{j_{\mathrm{prey}}}) G_{j_{\mathrm{pred}},j_{\mathrm{prey}},i_d}}_{\text{messy feeding}}$$

This surface production is redistributed throughout the water column as a depth dependent flux, F_{z,i_d}. To achieve this, F_{surface,i_d} is partitioned between a 'refractory' component (r^{POM}) that is predominantly remineralised close to the seafloor, and a 'labile' component ($1 - r^{\mathrm{POM}}$) which predominantly remineralises in the upper water column. The net remineralisation at depth z, relative to the

export depth z_0 is determined by characteristic length scales (l^{rPOM} and l^{POM} for 'refractory' and 'labile' POM respectively):

$$F_{z,i_d} = F_{\text{surface},i_d}\left[(1-r^{\text{POM}})\cdot\exp(\frac{z_0-z}{l^{\text{POM}}}) + r^{\text{POM}}\cdot\exp(\frac{z_0-z}{l^{\text{rPOM}}})\right] \quad (32)$$

The remineralisation length scales reflect a constant sinking speed and constant remineralisation rate. All POM reaching the seafloor is remineralised instantaneously. See Ridgwell et al. (2007a) for a fuller description and justification.

3.3.4 Coupling to BIOGEM

The calculations in BIOGEM are performed 48 times for each model year (i.e. once for every 2 time-steps taken by the ocean circulation mode). ECOGEM takes 20 time steps for each BIOGEM time-step i.e. 960 time-steps per year). At the beginning of each ECOGEM time-step loop, concentrations of inorganic tracers and key properties of the physical environment are passed from BIOGEM. The ecological community responds by transforming inorganic compounds into living biomass through photosynthesis. At the end of each ECOGEM time step loop, the rates of change in $\mathbf{R}$ and $\mathbf{OM}$ are passed back to BIOGEM. $\partial\mathbf{R}/\partial t$ is used to update DIC, phosphate, iron, oxygen and alkalinity tracers, while $\partial\mathbf{D}_1/\partial t$ is added to the dissolved organic matter pools. The rate of particulate organic matter production, $\partial\mathbf{D}_2/\partial t$ is instantly remineralised at depth using to the standard BIOGEM export functions described above (equation 32). $\frac{\partial\mathbf{B}}{\partial t}$ is used only to update the living biomass concentrations within ECOGEM. The structure of the coupling is illustrated in Figure 1.

In the initial implementation of ECOGEM described and evaluated here, the explicit plankton community is held entirely within the ECOGEM module and is not subject to physical transport (e.g. advection and diffusion) by the ocean circulation model (although dissolved tracers such as nutrients still are). As a first approximation, this approach appears to be acceptable, as long as the rate of transport between the very large grid cells in ~~cGENIE~~ cGEnIE is slow in relation to the net growth rates of the plankton community. On-line advection of ecosystem state variables will be implemented and its consequences explored in a future version of ~~EcoGENIE~~EcoGEnIE.

3.4 Ecophysiological parameterisation

The model community is made up of a number of different plankton populations, with each one described according to the same set of equations, as outlined above. Differences between the populations are specified according to individual parameterisation of the equations. In the following sections, we describe how the members of the plankton community are specified, and how their parameters are assigned according to the organism's size and taxonomic group.

3.4.1 Model structure

The plankton community in ECOGEM is designed to be highly configurable. Each population present in the initial community is specified by a single line in an input text file, which describes the organism size and taxonomic group.

In this configuration we include 16 plankton populations across eight different size classes. These are divided into two PFTs, namely, "Phytoplankton" and "Zooplankton" (see Table 2). The eight phytoplankton populations have nutrient uptake and photosynthesis traits enabled, and predation traits disabled, whereas the opposite is true for the eight zooplankton populations. In future we expect to bring in a wider range of trait-based functional types, including siliceous plankton (e.g. Follows et al., 2007), calcifiers (Monteiro et al., 2016), nitrogen fixers (Monteiro et al., 2010), and mixotrophs (Ward and Follows, 2016).

Table 2. Plankton functional groups and sizes in the standard run.

j	PFT	ESD (μm)	j	Functional Type	ESD (μm)
1	Phytoplankton	0.6	11	Zooplankton	0.6
2	Phytoplankton	1.9	12	Zooplankton	1.9
3	Phytoplankton	6.0	13	Zooplankton	6.0
4	Phytoplankton	19.0	14	Zooplankton	19.0
5	Phytoplankton	60.0	15	Zooplankton	60.0
6	Phytoplankton	190.0	16	Zooplankton	190.0
7	Phytoplankton	600.0	17	Zooplankton	600.0
8	Phytoplankton	1900.0	18	Zooplankton	1900.0

3.4.2 Size-dependent traits

With the exception of the maximum photosynthetic rate ($P_{\mathrm{C}}^{\max}$, see below), the size-dependent eco-physiological parameters (p) given in Table 3 are assigned as power-law functions of organismal volume ($V = \pi[ESD]^3/6$) according to standard equations of the form,

$$p = a\left(\frac{V}{V_0}\right)^b \tag{33}$$

Here V_0 is a reference value of V_0 = 1 μm^3. The value of p at $V = V_0$ is given by the coefficient a, while the rate of change in p as a function of V is described by the exponent b.

The maximum photosynthetic rate ($P_{\mathrm{C}}^{\max}$) of very small cells (i.e. $\lesssim$ 5 μm ESD) has been shown to deviate from the standard power law of equation 33 (Raven, 1994; Bec et al., 2008; Finkel et al., 2010), so we use the slightly more complex unimodal function given by Ward and Follows (2016).

$$P_{\mathrm{C}}^{\max} = \frac{p_a + \log_{10}(\frac{V}{V_0})}{p_b + p_c \log_{10}(\frac{V}{V_0}) + \log_{10}(\frac{V}{V_0})^2} \tag{34}$$

The parameters of this equation (listed in Table 3), were derived empirically from the data of Marañón et al. (2013).

Table 3. Size-dependent ecophysiological parameters (p) and their units, with size-scaling coefficients (a, b and c) for use in equations 33 and 34.

Parameter	Symbol	Size-scaling coefficients			Units
	p	a	b	c	
Inorganic nutrient uptake					
Maximum photosynthetic rate	$P_{\mathrm{C}}^{\max}$	3.08	5.00	-3.80	mmol N (mmol C)$^{-1}$ d^{-1}
Maximum nutrient uptake rates	$V_{\mathrm{PO_4}}^{\max}$	4.4×10^{-2}	0.06		mmol P (mmol C)$^{-1}$ d^{-1}
	$V_{\mathrm{Fe}}^{\max}$	1.4×10^{-4}	-0.09		mmol Fe (mmol C)$^{-1}$ d^{-1}
Nutrient affinities	$\alpha_{\mathrm{PO_4}}$	1.10	-0.35		m^3 (mmol C)$^{-1}$ d^{-1}
	α_{Fe}	0.175	-0.36		m^3 (mmol C)$^{-1}$ d^{-1}
Carbon quotas					
Cell carbon content	Q_{C}	1.45×10^{-11}	0.88		mmol C cell^{-1}
Grazing					
Maximum prey ingestion rate	G_{C}^{max}	21.9	-0.16		d^{-1}

3.4.3 Size-independent traits

A list of size-independent model parameters are listed in Table 4.

3.5 Parameter modifications

As far as possible, the parameter values applied in ECOGEM were kept as close as possible to previously published versions of the model (Ward and Follows, 2016). There were however a few modifications that were required to bring ~~EcoGENIE~~ EcoGEnIE into first order agreement with observations and the current version of ~~cGENIE~~ cGEnIE (Ridgwell and Death, in prep.). In particular, in comparison to the biogeochemical model used in Ward and Follows (2016), the amount of soluble iron supplied to ~~cGENIE~~ cGEnIE by atmospheric deposition is considerably less. With a smaller source of iron, it was necessary to decrease the iron demand of the plankton community, and this was achieved by decreasing $Q_{\mathrm{Fe}}^{\max}$ and $Q_{\mathrm{Fe}}^{\min}$ by five-fold ($Q_{\mathrm{Fe}}^{\max}$ from 20 to 4 nmol Fe (mmol C)$^{-1}$, and $Q_{\mathrm{Fe}}^{\min}$ from 5 to 1 nmol Fe (mmol C)$^{-1}$).

We also found that the flexible stoichiometry of ECOGEM led to excessive export of carbon from the surface ocean, attributable to higher C:P ratios in organic matter (BIOGEM assumes a Redfieldian C:P of 106). This effect was moderated by ~~adding the respiration term, which returns a fraction of carbon biomass directly to DIC (it is assumed that other elements are not lost in this way)~~increasing the size of the minimum phosphate:carbon quota, $Q_{\mathrm{P}}^{\min}$ (relative to Ward et al., 2012) . The additional production of POC also led to increased production of calcium carbonate. This was counteracted by increasing the PIC:POC production ratio ($r^{\mathrm{CaCO_3:POC}}$) from 0.022 to 0.0285,

Table 4. Size-independent model parameters.

Parameter	Symbol	Value	Units
Nutrient quotas			
Minimum phosphate:carbon quota	$Q_{\mathrm{P}}^{\mathrm{min}}$	~~2.1~~3.3$\times 10^{-3}$	mmol P (mmol C)$^{-1}$
Maximum phosphate:carbon quota	$Q_{\mathrm{P}}^{\mathrm{max}}$	1.1$\times 10^{-2}$	mmol P (mmol C)$^{-1}$
Minimum iron:carbon quota	$Q_{\mathrm{Fe}}^{\mathrm{min}}$	1.0$\times 10^{-6}$	mmol Fe (mmol C)$^{-1}$
Maximum iron:carbon quota	$Q_{\mathrm{Fe}}^{\mathrm{max}}$	4.0$\times 10^{-6}$	mmol Fe (mmol C)$^{-1}$
Temperature			
Reference temperature	T_{ref}	20	°C
Temperature dependence	A	0.05	-
Photosynthesis			
Maximum Chl-*a*-to-phosphorus ratio	$\theta_{\mathrm{N}}^{\mathrm{max}}$	48	mg Chl *a* (mmol P)$^{-1}$
Initial slope of P-I curve	α	3.83$\times 10^{-7}$	mmol C (mg Chl *a*)$^{-1}$(μEin m^{-2})$^{-1}$
Cost of biosynthesis	ξ	37.28	mmol C (mmol P)$^{-1}$
Grazing			
Optimum predator:prey length ratio	ϑ_{opt}	10	-
Geometric s.d. of ϑ	σ_{graz}	2.0	-
Total prey half-saturation	$k_{\mathrm{C}}^{\mathrm{prey}}$	5.0	mmol C m^{-3}
Maximum assimilation efficiency	λ^{max}	0.7	-
Grazing refuge parameter	Λ	-1	(mmol C m^{-3})$^{-1}$
Active switching parameter	s	2	-
Assimilation shape parameter	h	0.1	-
Other loss terms			
Plankton mortality	m	0.05	d^{-1}
~~Plankton respiration~~	~~$r_{i_b=\mathrm{DIC}}$ 0.05 d^{-1}~~ $r_{i_b\neq\mathrm{DIC}}$	0	d^{-1}
Partitioning of organic matter			
Fraction to DOM	β	0.66	-
Light attenuation			
Light attenuation by water	k_{w}	0.04	m^{-1}
Light attenuation by chlorophyll	k_{Chl}	0.03	m^{-1}(mg Chl)$^{-1}$

and decreasing the thermodynamic calcification rate power (η) from 1.28 to 0.744 (Ridgwell et al., 2007a).

4 Simulations and Data

4.1 10,000 year spin-up

We ran ~~eGENIE~~ cGEnIE (as configured and described in Ridgwell and Death, in prep.) and ~~EcoGENIE~~ EcoGEnIE (as described here) each for period of 10,000 years. These runs were initialised from a homogenous and static ocean, with an imposed constant atmospheric CO_2 concentration of 278 ppm. We present model output from the 10,000th year of integration.

4.2 Observations

Although they are not necessarily strictly comparable, we compare results from the pre-industrial configurations of ~~eGENIE and EcoGENIE~~ cGEnIE and EcoGEnIE to contemporary climatologies from a range of sources. Global climatologies of dissolved phosphate and oxygen are drawn from the World Ocean Atlas ~~(WOA~~ 2009 ~~)~~(WOA09 - Garcia et al., 2010), while DIC and alkalinity are taken from Global Ocean Data Analysis Project ~~(GLODAP)~~version 2 (GLODAPv2 - **?**). Surface chlorophyll concentrations represent a climatological average from 1997 to 2002, estimated by the SeaWiFS satellite. Depth-integrated primary production is from Behrenfeld and Falkowski (1997). All of these interpolated global fields have been re-gridded onto the ~~eGENIE~~ cGEnIE 36×36×16 grid.

Observed dissolved iron concentrations are those published by Tagliabue et al. (2012). These data are too sparse and variable to allow reliable mapping on the ~~eGENIE~~ cGEnIE grid, and are therefore shown as individual data.

Fidelity to the observed seasonal cycle of nutrients and biomass was evaluated against observations from nine Joint Global Ocean Flux Study (JGOFS) sites: the Hawai'i Ocean Time-series (HOT: 23°N, 158°W), the Bermuda Atlantic Time-series Study (BATS: 32°N, 64°W), the equatorial Pacific (EQPAC: 0°N, 140°W), the Arabian Sea (ARABIAN: 16°N, 62°E), the North Atlantic Bloom Experiment (NABE: 47°N, 19°W), Station P (STNP: 50°NS, 145°W), Kerfix (KERFIX: 51°S, 68°E), Antarctic Polar Frontal Zone (APFZ: 62°S, 170°W) and the Ross Sea (ROSS: 75°S, 180°W). Model output for KERFIX and the Ross Sea site was not taken at the true locations of the observations (51°S, 68°E and 75°S, 180°W, respectively). Kerfix was moved to compensate for a poor representation of the Polar Front within the coarse resolution ocean model, while the Ross Sea site does not lie within the GEnIE ocean grid. At each site, the observational data represent the mean daily value within the mixed layer. Observational data from all years are plotted together as one climatological year.

5 Results

5.1 Biogeochemical variables

We start by describing the global distributions of key biogeochemical tracers that are common to both ~~cGENIE and EcoGENIE~~cGEnIE and EcoGEnIE.

5.1.1 Global surface values

Annual mean global distributions are presented for the upper 80.8 m of the water column, corresponding to the model surface layer. In Figure 2 we compare output from the two models to observations of dissolved phosphate and iron. Surface phosphate concentrations are broadly similar between the two versions of the model, except that ~~EcoGENIE~~ EcoGEnIE provides slightly lower estimates in the Southern Ocean and equatorial upwellings. Both versions strongly underestimate surface phosphate in the equatorial and north Pacific, and to a lesser extent in the north and east Atlantic, the Arctic and the Arabian Sea. This is likely attributable in part to the model underestimating the strength of upwelling in these regions. It should also be noted that the observations may in some cases be unrepresentative of the true surface layer, when this is significantly shallower than 80.8 m. In such cases the observed value will be affected by measurements from below the surface layer. Iron distributions are also broadly similar between the two models, with ~~EcoGENIE~~ EcoGEnIE showing slightly lower iron concentrations over most of the ocean.

Figure 3 shows observed and modelled values of inorganic carbon, oxygen and alkalinity. The two models yield very similar surface distributions of the three tracers. DIC and alkalinity are both broadly underestimated relative to observations, while oxygen shows higher fidelity, albeit with artificially high estimates in the equatorial Atlantic and Pacific. This is likely attributable to unrealistically weak upwelling in these regions.

Surface ΔpCO_2 from the two models is shown in Figure 4. ~~EcoGENIE~~ EcoGEnIE shows weaker CO_2 outgassing in the tropical band, with a much stronger ocean-to-atmosphere flux in the Western Arctic.

In Figure 5 we show the annual mean rate of particulate organic matter production in the surface layer, and the relative differences between ECOGEM and BIOGEM. In comparison to ~~cGENIE, EcoGENIE~~ cGEnIE, EcoGEnIE shows elevated POC production in all regions. Production of $CaCO_3$ is globally less variable in ~~EcoGENIE than cGENIE~~EcoGEnIE than cGEnIE, with notable higher fluxes in the oligotrophic gyres and polar regions.

The relative proportions in which these elements and compounds are exported from the surface ocean are regulated by the stoichiometry of biological production. In ~~cGENIE~~ cGEnIE (BIOGEM), carbon and phosphorus production are rigidly coupled through a fixed ratio of 106:1, while POFe:POC and $CaCO_3$:POC ~~production~~ export flux ratios are regulated as a function of environmental conditions. In ~~ecoGENIE~~ ecoGEnIE (ECOGEM), phosphorus, iron and carbon ~~production~~

fluxes are all decoupled through the flexible quota physiology, which depends on both environmental conditions, and the status of the food-web. Only $CaCO_3$:POC ~~production~~ flux ratios are regulated via the same mechanism in the two models (although we decreased the average $CaCO_3$:POC ratio in ECOGEM to compensate for the elevated POC production relative to POP).

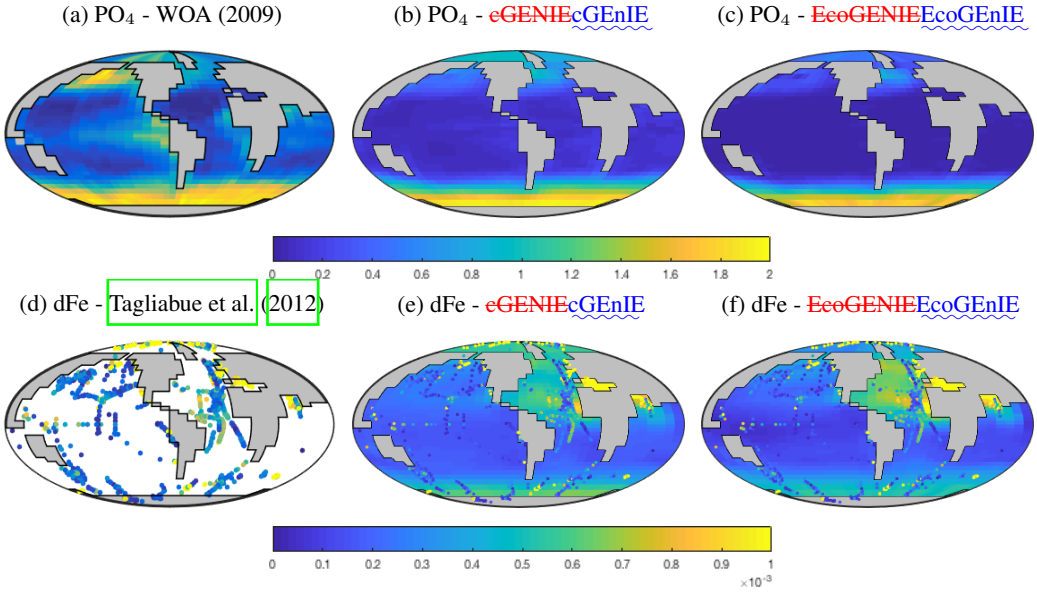

Figure 2. Surface concentrations of dissolved ~~inorganic nutrients~~phosphate (mmol PO_4 m^{-3}) and iron (mmol dFe m^{-3}).

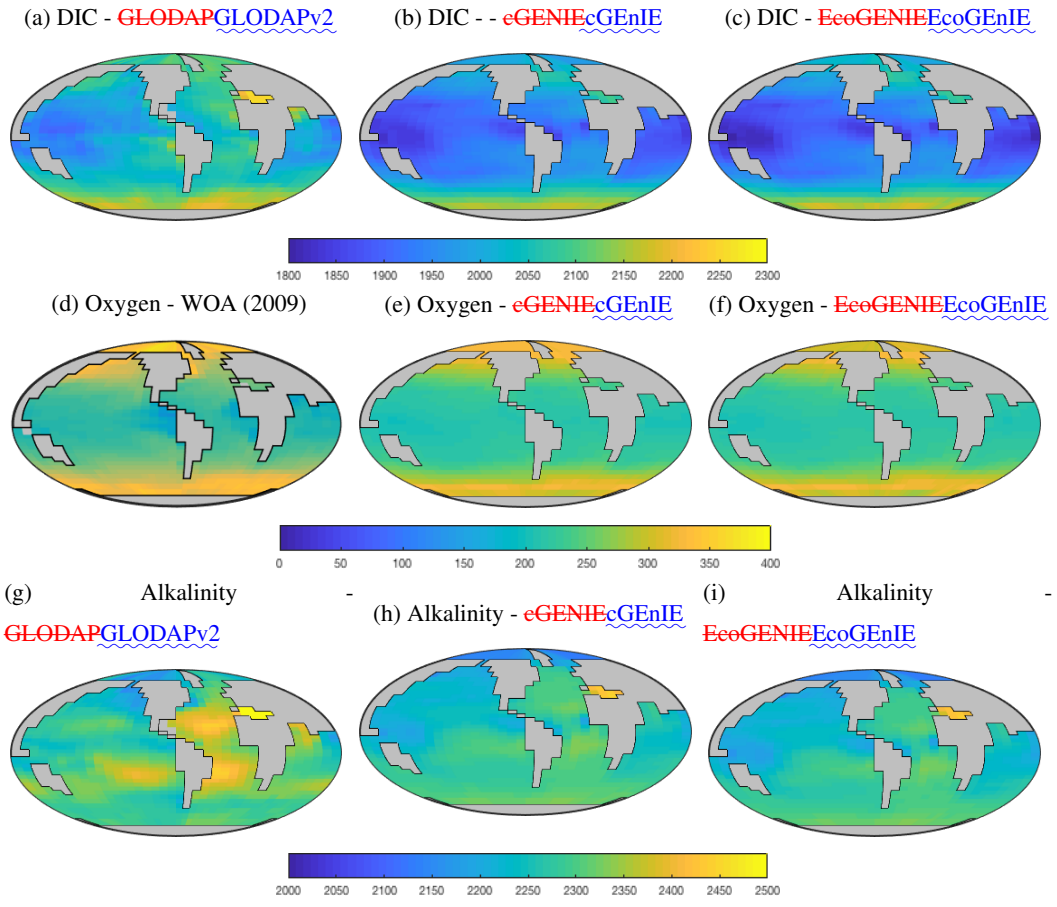

Figure 3. Surface concentrations of dissolved inorganic carbon (mmol C m^{-3}), alkalinity (meq m^{-3}) and dissolved oxygen (mmol O_2 m^{-3}).

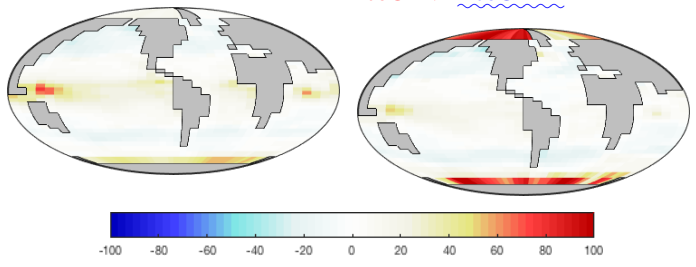

Figure 4. (Preindustrial) surface ΔpCO_2 (ppm).

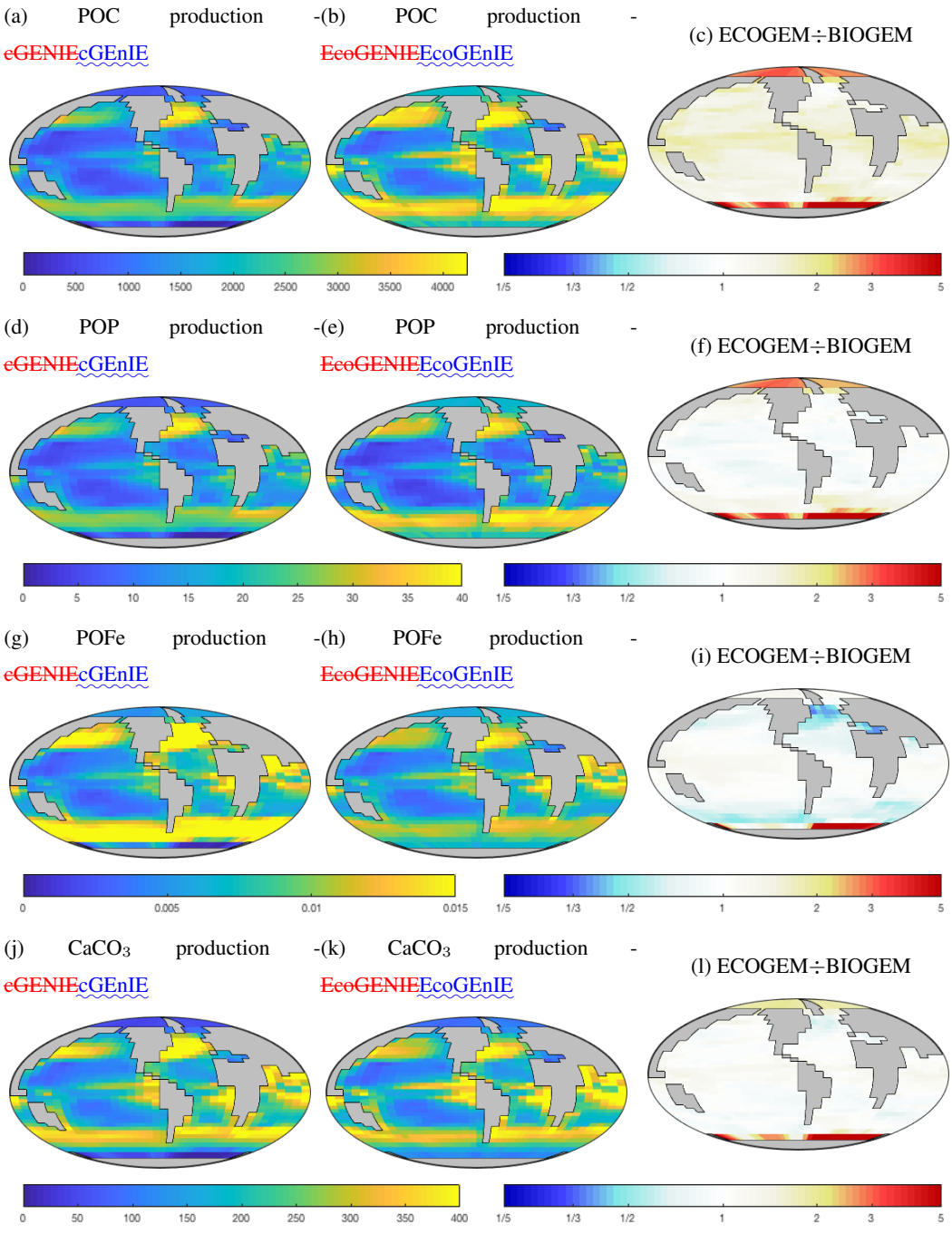

Figure 5. ~~Particulate matter production~~ Vertical fluxes of particulate carbon (mmol C m^{-2} d^{-1}), phosphorus (mmol P m^{-2} d^{-1}), iron (mmol Fe m^{-2} d^{-1}) and ~~export from~~ calcium carbonate (mmol $CaCO_3$ m^{-2} d^{-1}) across the base of the surface layer~~)~~. The right-hand column indicates the relative increase or decrease in ECOGEM, relative to BIOGEM (dimensionless).

5.1.2 Basin-averaged depth profiles

In this section we present the meridional depth distributions of key biogeochemical tracers, averaged across each of the three main ocean basins, as shown in Figure 6. Figure 7 shows that the distribution of dissolved phosphate is very similar between the two models, with ~~EcoGENIE~~ EcoGEnIE showing a slightly stronger sub-surface accumulation in the northern Indian Ocean.

The vertical distributions shown in Figure 8 reveal that dissolved iron is lower throughout the ocean in ~~EcoGENIE~~EcoGEnIE, relative to ~~cGENIE~~cGEnIE, particularly below 1500 m. Differences are less obvious at intermediate depths. (Observations are currently too sparse to estimate reliable basin-scale distributions of dissolved iron; see Tagliabue 2016.)

Figure 9 shows that while ~~cGENIE~~ cGEnIE reproduces observed DIC distributions very well, ~~EcoGENIE~~ EcoGEnIE overestimates concentrations within the Indian and Pacific Oceans. The total oceanic DIC inventory increased by just under 2% from ~~0.299 mol C in cGENIE to 0.304 in EcoGENIE~~ 2.99 Examol C in cGEnIE to 3.05 in EcoGEnIE (with a fixed atmospheric CO_2 concentration of 278 ppm). Otherwise the two models show broadly similar distributions, with the most pronounced differences (as for PO_4) in the northern Indian Ocean.

Figure 10 shows that ~~cGENIE~~ cGEnIE reasonably captures the invasion of O_2 into the ocean interior through the Southern Ocean and North Atlantic. These patterns are also seen in ~~EcoGENIE~~EcoGEnIE, although unrealistic water column anoxia is seen in the northern intermediate Indian and Pacific Oceans. Again, this is likely a consequence of greater export and remineralisation of organic carbon in ~~EcoGENIE~~EcoGEnIE, leading to more oxygen consumption at intermediate depths (also evidenced by elevated PO_4, DIC and alkalinity in the same regions; Figures 7, 9 and 11).

Alkalinity (Figure 11) also shows some clear differences between the two models, again most noticeably in the northern intermediate Indian and Pacific Oceans. In these regions ~~EcoGENIE~~ EcoGEnIE shows excessive accumulation of alkalinity at ~1000 m depth. This is again attributable to the increased C export in ~~EcoGENIE~~EcoGEnIE. In the absence of a nitrogen cycle (and NO_3^- reduction), increased anoxic remineralisation of organic carbon (Figures 9 and 10) leads to increased reduction of sulphate to H_2S, which in turn increases the alkalinity of seawater. Further adjustment of the ~~respiration of carbon~~ cellular nutrient quotas in ECOGEM and hence the effective exported P:C Redfield ratio, and/or retuning of the organic matter remineralisation profiles in BIOGEM (Ridgwell et al., 2007a) would likely resolve these issues.

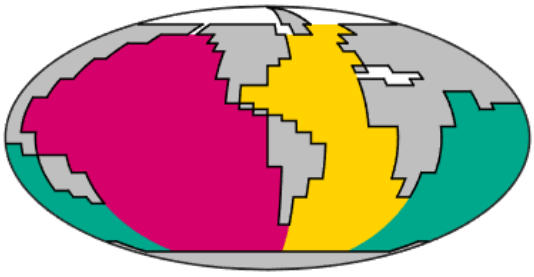

Figure 6. Spatial definition of the three ocean basins used in Figures 7 to 10. Locations of the JGOFS time-series sites are indicated with blue dots.

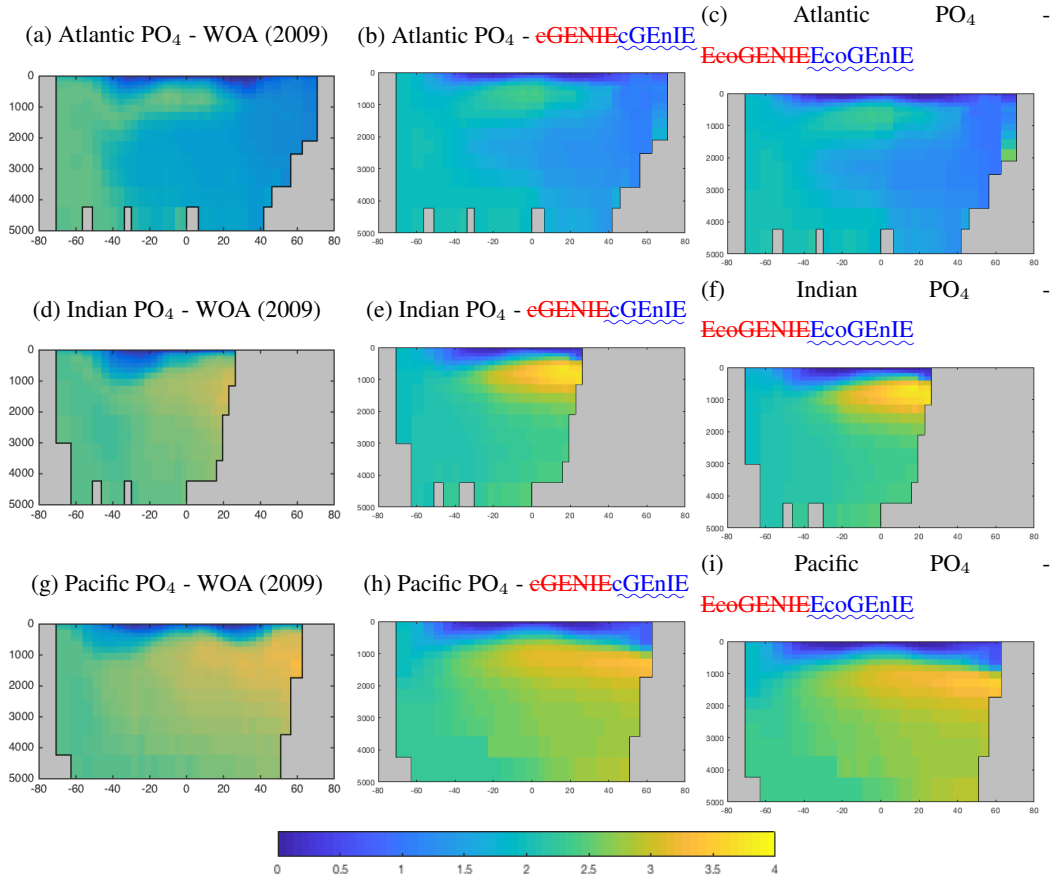

Figure 7. Basin-averaged meridional-depth distribution of phosphate (mmol P m^{-3}).

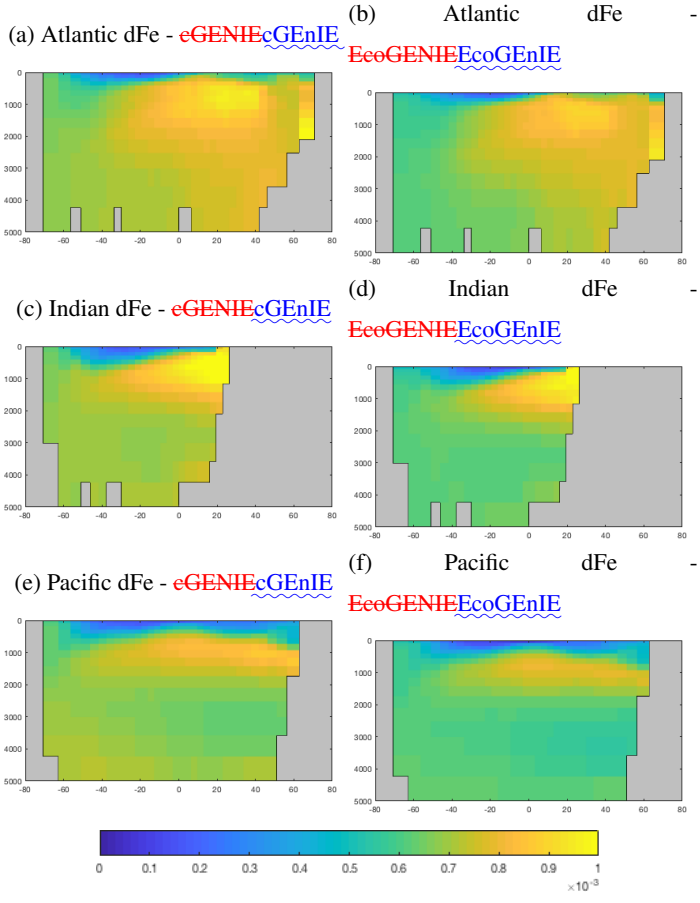

Figure 8. Basin-averaged meridional-depth distribution of total dissolved iron (mmol dFe m^{-3}).

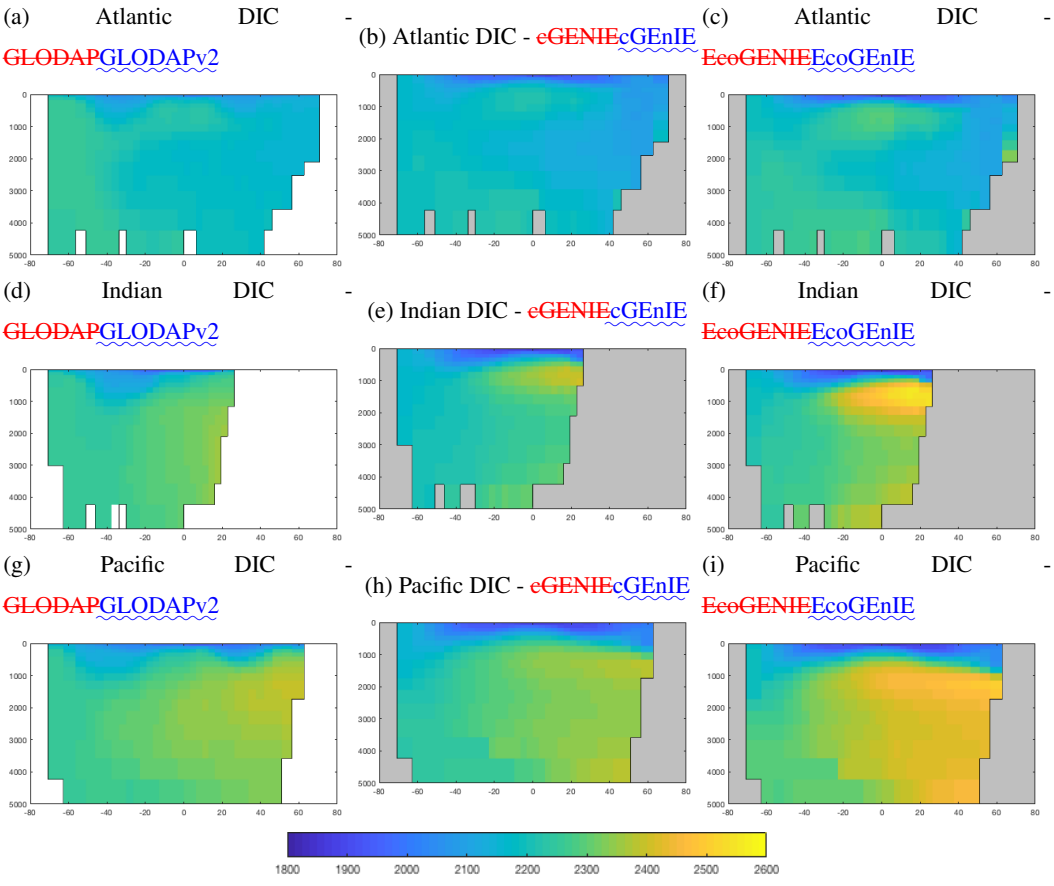

Figure 9. Basin-averaged meridional-depth distribution of DIC (mmol C m^{-3}).

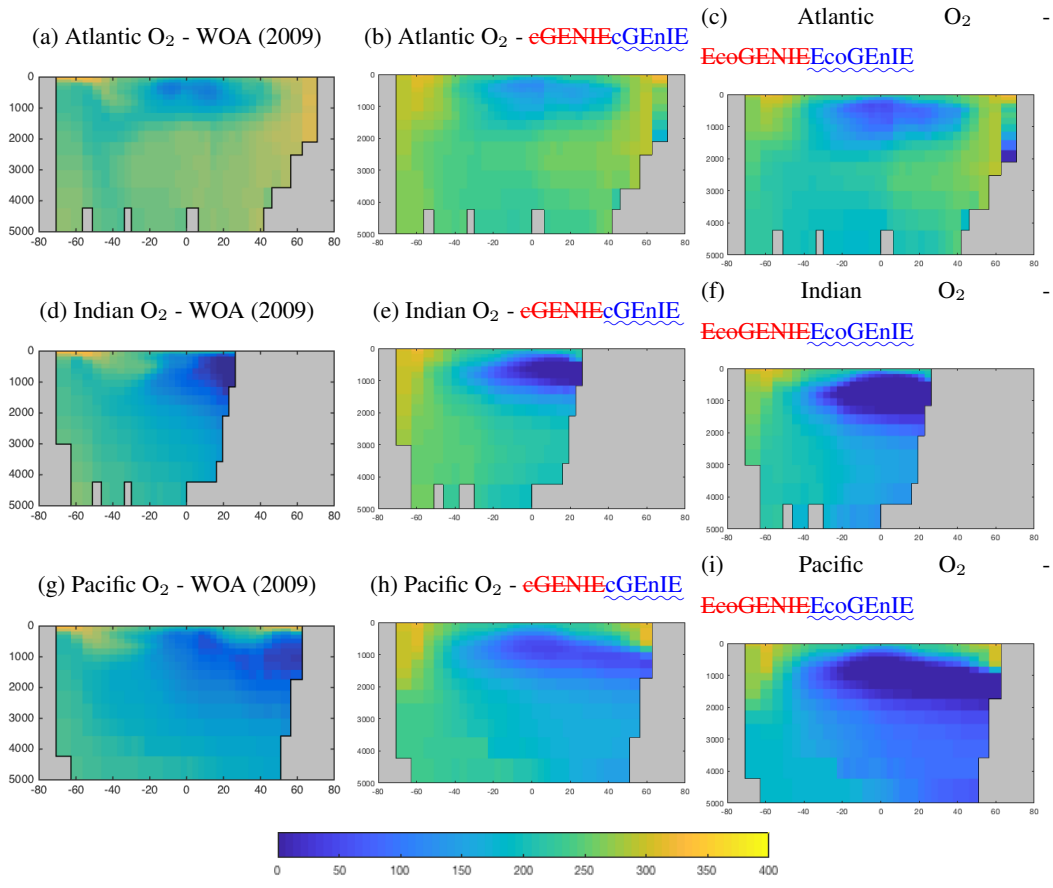

Figure 10. Basin-averaged meridional-depth distribution of dissolved oxygen (mmol O_2 m^{-3}).

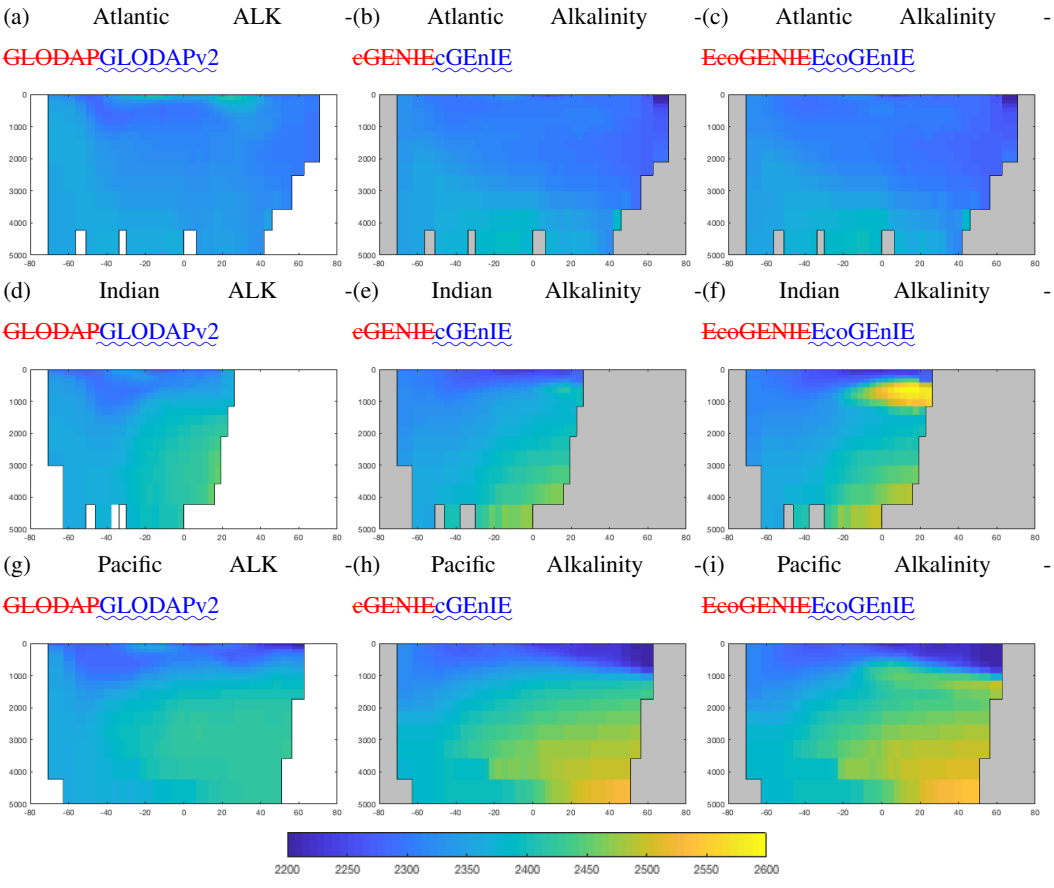

Figure 11. Basin-averaged meridional-depth distribution of alkalinity (meq m^{-3}).

5.1.3 Time-series

Figures 12 and 13 ~~we~~ compare the seasonal cycles of surface nutrients (phosphate and iron) at nine Joint Global Ocean Flux Study (JGOFS) sites.

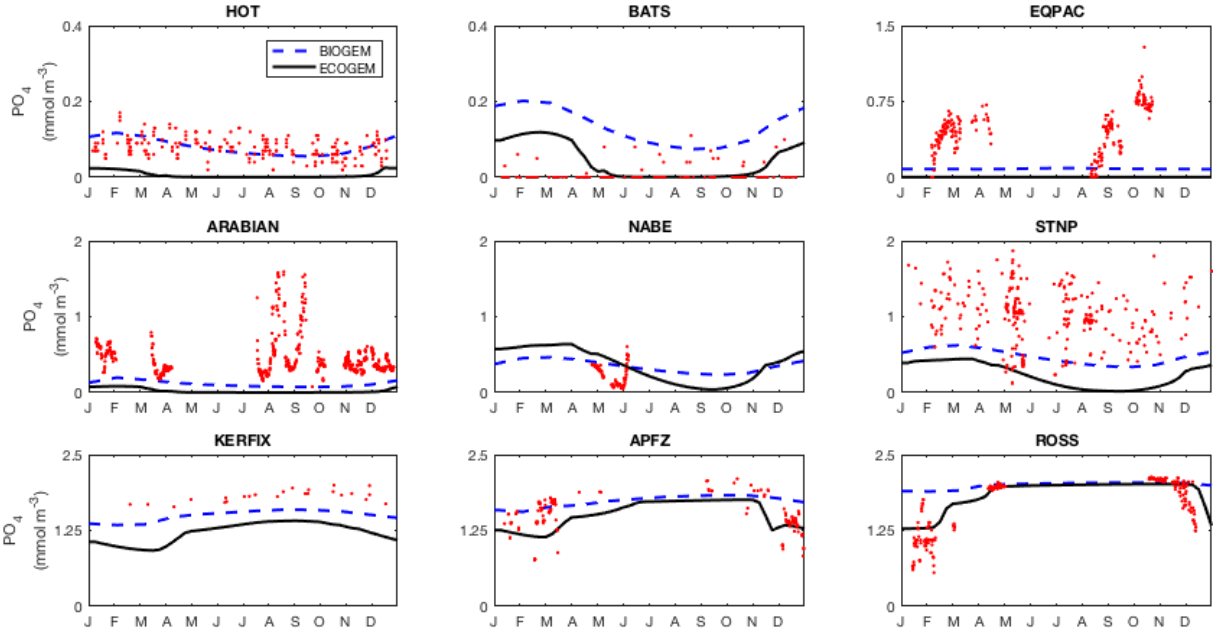

Figure 12. Annual cycle of surface PO_4 at 9 time-series sites in ~~cGENIE~~ cGEnIE and ~~EcoGENIE~~EcoGEnIE. Red dots indicate climatological observations, while the lines represent modelled surface PO_4 concentrations. Locations of the time-series are indicated in Figure 6.

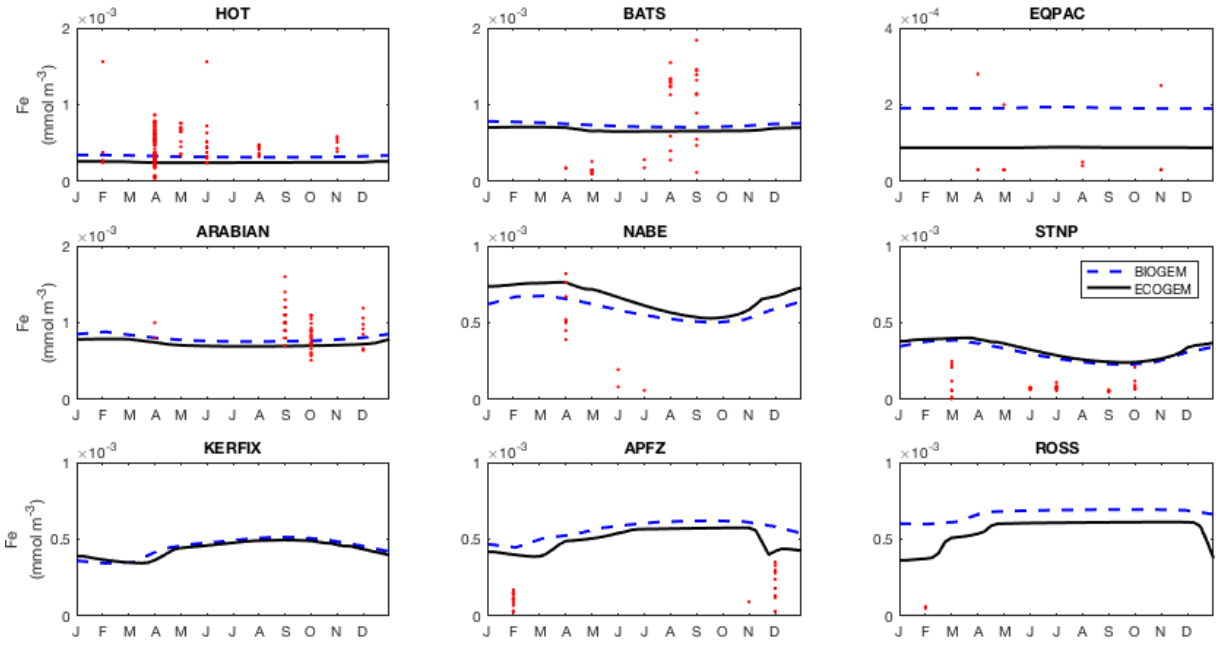

Figure 13. Annual cycle of surface dissolved iron at 9 time-series sites in ~~eGENIE~~ cGEnIE and ~~EcoGENIE~~EcoGEnIE. Red dots indicate climatological observations, while the lines represent modelled surface iron concentrations. Locations of the time-series are indicated in Figure 6.

5.2 Ecological variables

Moving on from the core components that are common to both models, we present a range of ecological variables that are exclusive to ~~EcoGENIE~~EcoGEnIE. As before, we begin by presenting the annual mean global distributions in the ocean surface layer, comparing total chlorophyll and primary production to satellite-derived estimates (Figure 14). We then look in more detail at the community composition, with Figure 15 showing the carbon biomass within each plankton population. Figure 16 then shows the degree of nutrient limitation within each phytoplankton population. Finally, in Figure 17, we show the seasonal cycle of community and population level chlorophyll at each of the nine JGOFS time-series sites.

5.2.1 Global surface values

Figure 14 reveals that ~~EcoGENIE~~ EcoGEnIE shows some limited agreement with the satellite-derived estimate of global chlorophyll. As expected, chlorophyll biomass is elevated in the high-latitude oceans relative to lower latitudes. The sub-tropical gyres show low biomass, but the distinction with higher latitudes is not as clear as in the satellite estimate. The model also shows a clear lack of chlorophyll in equatorial and coastal upwelling regions, relative to the satellite estimate. The model predicts higher chlorophyll concentrations in the Southern Ocean than the satellite estimate, although it should be noted that the satellite algorithms may be underestimating concentrations in these regions (~~Dierssen, 2010~~)(Figure 17 and Dierssen, 2010).

Modelled primary production correctly increases from the oligotrophic gyres towards high latitudes and upwelling regions, but variability is much lower than in the satellite estimate. Specifically, the model and satellite estimates yield broadly similar estimates in the oligotrophic gyres, but the model does not attain the high values seen at higher latitudes and in coastal areas.

Figure 15 shows the modelled carbon biomass concentrations in the surface layer, for each modelled plankton population. The smallest (0.6 μm) phytoplankton size class is evenly distributed in the low-latitude oceans between 40° N and S, but is largely absent nearer to the poles. The 1.9 μm phytoplankton size class is similarly ubiquitous at low latitudes, albeit with somewhat higher biomass, and its range extends much further towards the poles. With increasing size, the larger phytoplankton are increasingly restricted to highly productive areas, such as the sub-polar gyres and upwelling zones.

Perhaps as expected, zooplankton size classes tend to mirror the biogeography of their phytoplankton prey. The smallest (1.9 μm) surviving size class is found primarily at low latitudes, although a highly variable population is found at higher latitudes. This population is presumably supported by grazing on the larger 6 μm size class (with very low efficiency dictated by the unfavourable predator-prey length ratio). Larger zooplankton size classes follow a similar pattern to the phytoplankton,

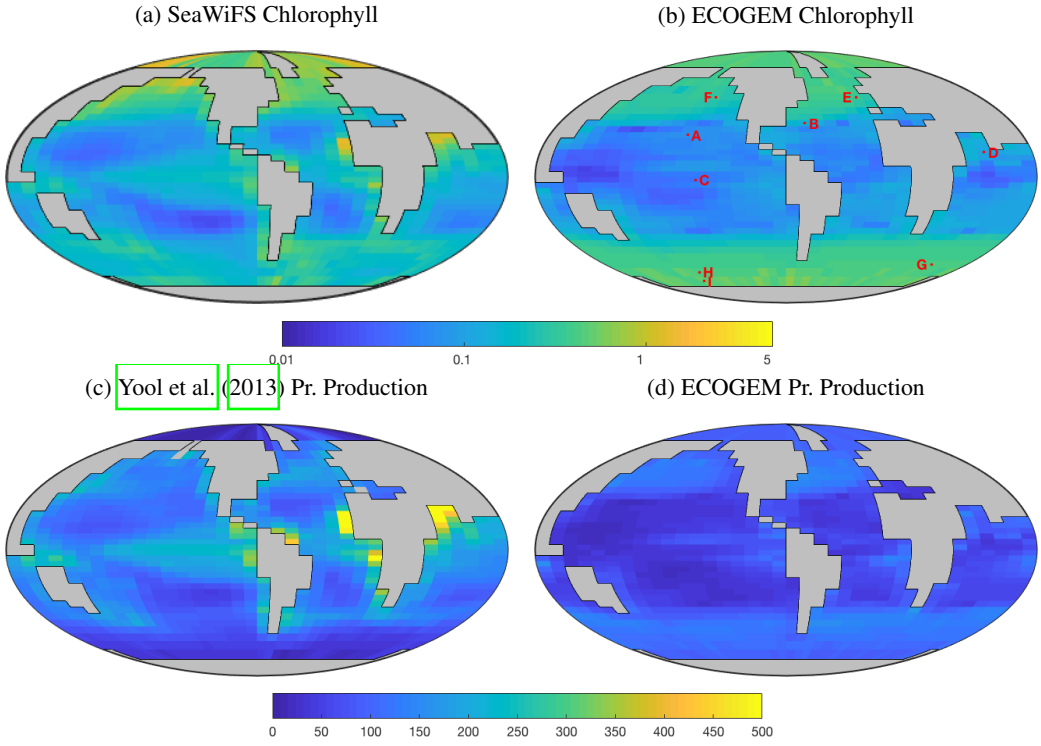

Figure 14. Satellite-derived (left) and modelled (right) surface chlorophyll *a* concentration (mg Chl m^{-3}) and depth-integrated primary production (mg C m^{-2} d^{-1}). The satellite-derived estimate of primary production is a composite of three products (Behrenfeld and Falkowski, 1997; Carr et al., 2006; Westberry et al., 2008), as in Yool et al. (2013, their Figure 12).

moving from a cosmopolitan but homogenous distribution in the smaller size classes, towards spatially more variable distributions among the larger organisms.

The degree of nutrient limitation within each phytoplankton size class is shown in Figure 16. The two-dimensional colour-scale indicates decreasing iron limitation from left to right, and decreasing phosphorus limitation from bottom to top. White is therefore nutrient replete, blue is phosphorus limited, red is iron limited, and magenta is phosphorus-iron co-limited. The figure demonstrates that the smallest size class is not nutrient limited in any region. The increasing saturation of the colour scale in larger size classes indicates an increasing degree of nutrient limitation. As expected, nutrient limitation is strongest in the highly stratified low latitudes. A stronger vertical supply of nutrients at higher latitudes is associated with weaker nutrient limitation, although nutrient limitation is still significant among the larger size classes. Consistent with observations (Moore et al., 2013), phosphorus limitation is restricted to low latitudes. Iron limitation dominates in high latitude regions. ~~Among the~~ , especially among larger size classes. Among these larger groups, the upwelling zones appear to be characterised by iron-phosphorus co-limitation.

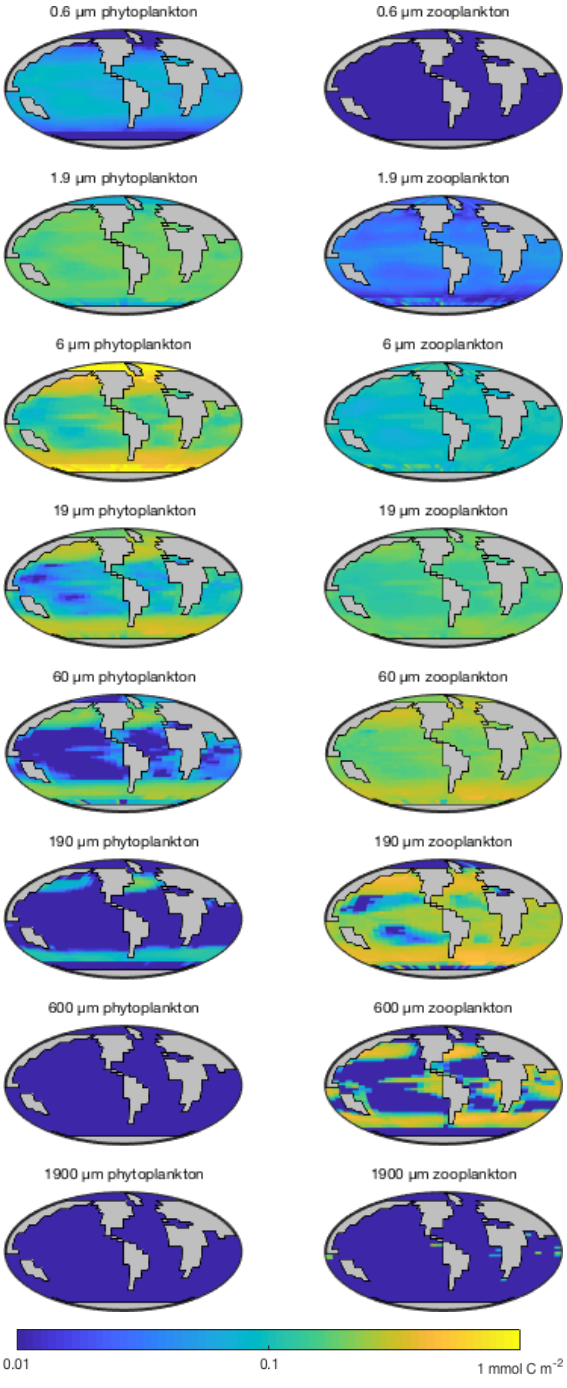

Figure 15. Surface concentrations of carbon biomass in each population (mmol C m^{-3}).

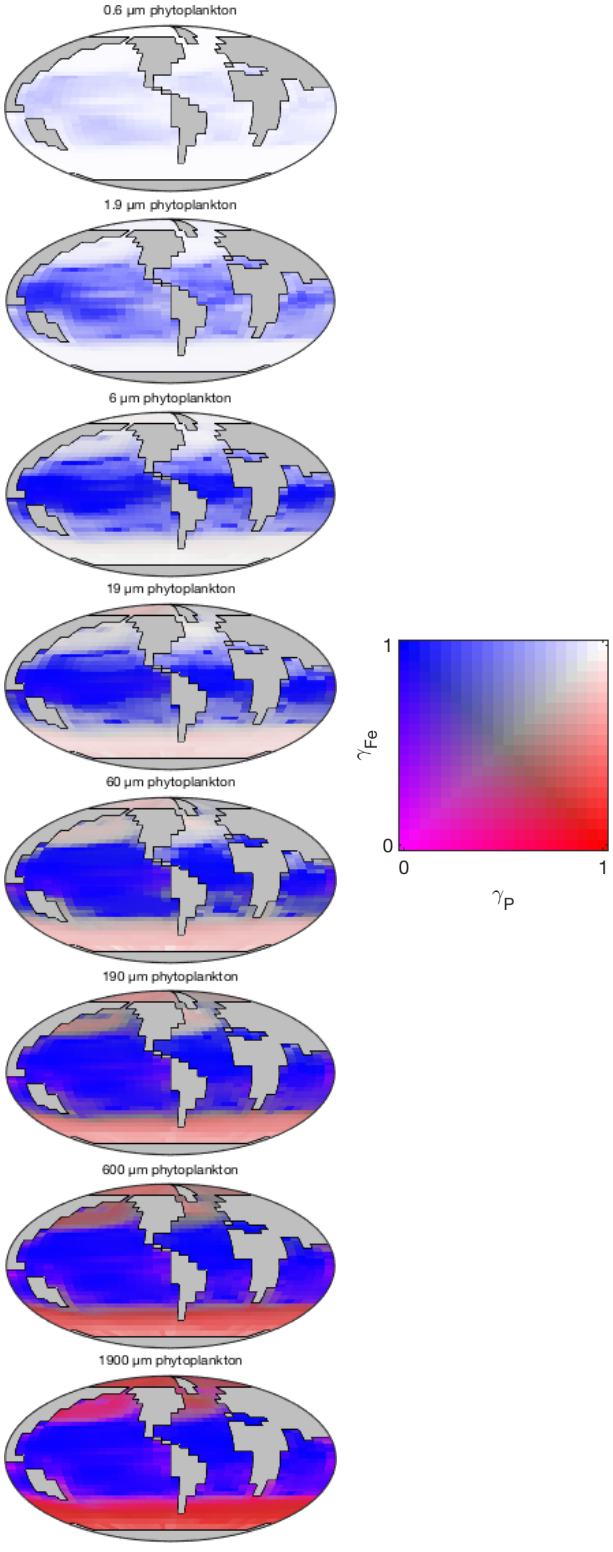

Figure 16. Nutrient limitation in each phytoplankton population (dimensionless). The two-dimensional colour-scale indicates decreasing phosphorus limitation from left to right, and decreasing iron limitation from bottom to top. White is therefore nutrient replete, blue is phosphorus limited, red is iron limited, and magenta is phosphorus-iron co-limited.

5.2.2 Time-series

The seasonal cycles of phytoplankton chlorophyll *a* are compared to time-series observations in Figure 17. The modelled total chlorophyll concentrations (black lines) track the observed concentrations (red dots) reasonably well at most sites~~, and perhaps better than might be expected from the comparison to satellite data~~. The bottom three panels also suggest that the satellite data shown in Figure 14 may slightly underestimate surface chlorophyll concentrations in the Southern Ocean. The modelled surface chlorophyll concentration is ~~probably~~ too low in the equatorial Pacific, while the spring bloom occurs one to two months earlier than was seen during the North Atlantic Bloom Experiment.

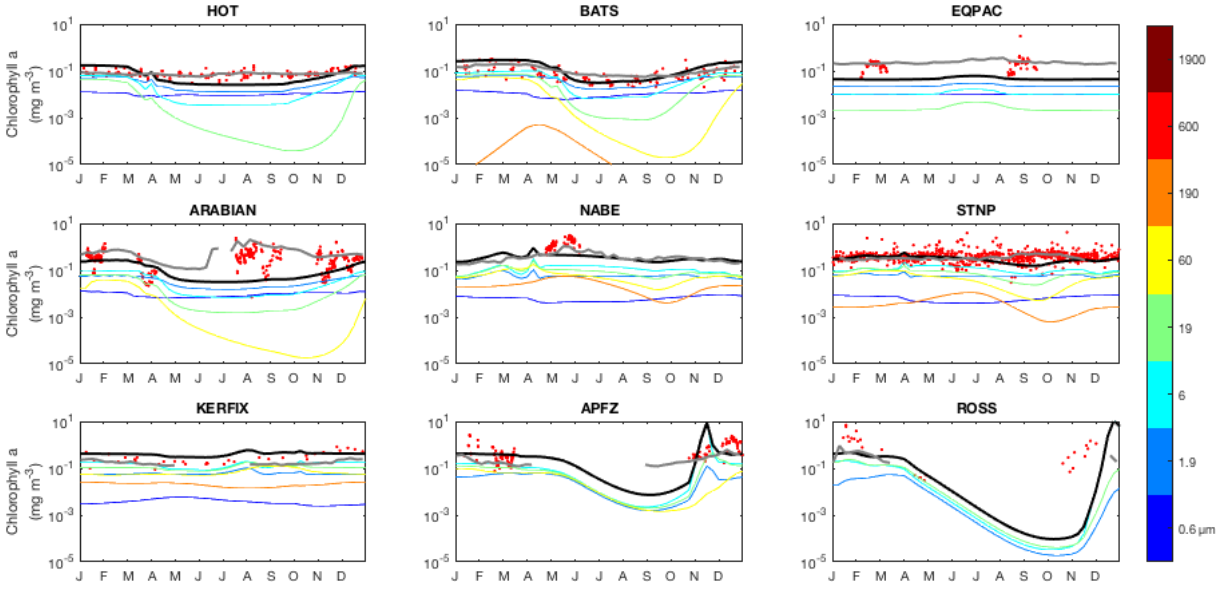

Figure 17. Annual cycle of surface chlorophyll *a* at nine JGOFS time-series sites. Red dots indicate climatological observations, while the black lines represents modelled total surface chlorophyll *a*. Coloured lines represent chlorophyll *a* in individual size classes (blue = small, red = large). Locations of the time-series are indicated in Figure 6. Satellite estimates of chlorophyll *a* are shown in grey.

The seasonal cycles of primary production in the surface layer are compared to time-series observations in Figure 18. As also indicated in Figure 14, the spatial variance in modelled primary production is too low, with primary production overestimated at the most oligotrophic site (HOT) and typically underestimated at the most productive sites (esp. the equatorial Pacific, NABE and the Ross Sea). In contrast to the lack of spatial variability, the model exhibits significant seasonal variation, often in excess of the observed variability (at those sites where the seasonal cycle is well resolved).

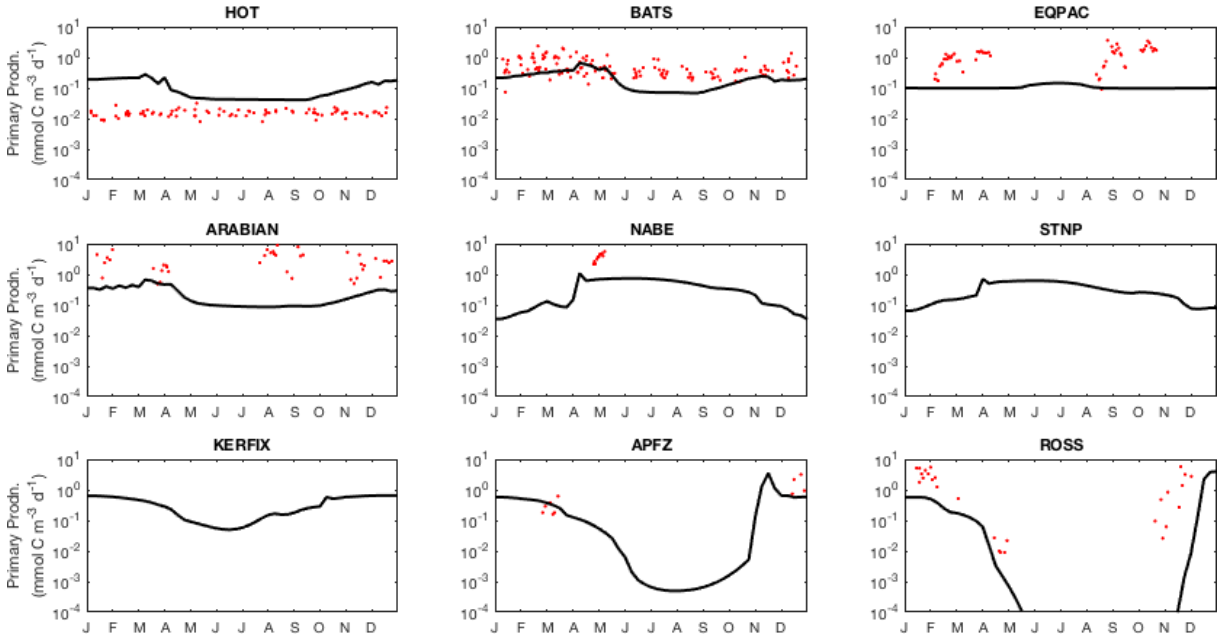

Figure 18. Annual cycle of surface primary production at nine JGOFS time-series sites. Red dots indicate climatological observations, while the black lines represents modelled total primary production. Locations of the time-series are indicated in Figure 6.

5.2.3 ~~eGENIE~~ cGEnIE vs. ~~EcoGENIE~~EcoGEnIE

Figure 19 is a Taylor diagram comparing the two models in terms of their correlation to observations and their standard deviations, relative to observations. A perfect model would be located at the middle of the bottom axis, with a correlation coefficient of 1.0 and a normalised standard deviation of 1.0. The closer a model is to this ideal point, the better a representation of the data it provides. Figure 19 shows that ~~EcoGENIE~~ EcoGEnIE is located further from the ideal point than ~~eGENIE~~cGEnIE, in terms of oxygen, alkalinity, phosphate, and DIC. The new model seems to provide a universally worse representation of global ocean biogeochemistry. This is perhaps not surprising, given that the BIOGEM component of ~~eGENIE~~ cGEnIE has at various times been systematically tuned to match the observation data (e.g. Ridgwell et al., 2007a; Ridgwell and Death, in prep.). ~~EcoGENIE~~ EcoGEnIE has not yet been optimised in this way.

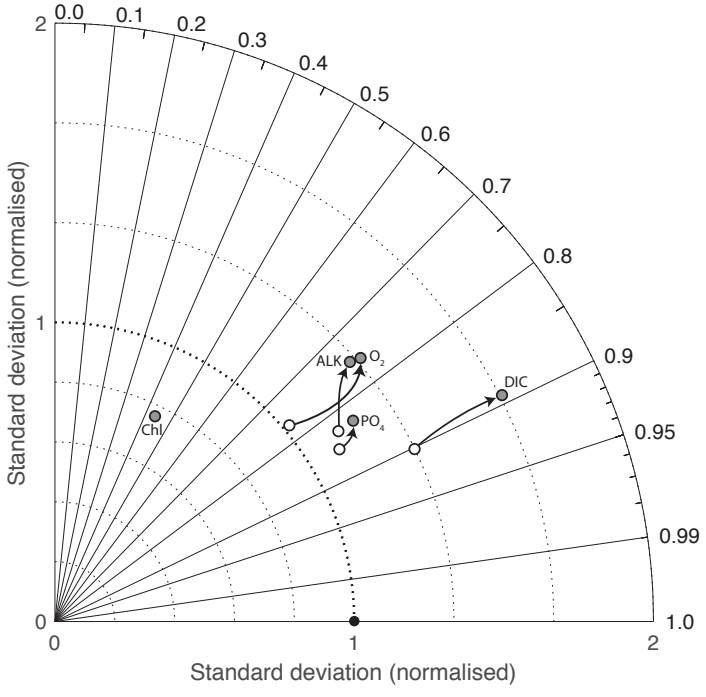

Figure 19. Taylor diagram comparing ~~eGENIE~~ cGEnIE (white dots) and ~~EcoGENIE~~ EcoGEnIE (grey dots) to annual mean observation fields.

6 Discussion

The marine ecosystem is a central component of the Earth system, harnessing solar energy to sustain the biogeochemical cycling of elements between dissolved inorganic nutrients, living biomass and decaying organic matter. The interaction of these components with the global carbon cycle is critical to our interpretation of past, present and future climates, and has motivated the development of a wide range of models. These can be placed on a spectrum of increasing complexity, from simple and computationally efficient box models to fully coupled Earth system models with extremely large computational ~~overheads~~costs.

~~cGENIE~~ cGEnIE is a model of intermediate complexity on this spectrum. It has been designed to allow rapid model evaluation while at the same time retaining somewhat realistic global dynamics that facilitate comparison with observations. With this goal in mind, the biological pump was parameterised as a simple vertical flux defined as a function of environmental conditions (Ridgwell et al., 2007a). This simplicity is well suited to questions concerning the interactions of marine biogeochemistry and climate, but at the same time precludes any investigation of the role of ecological interactions with the broader Earth system.

Here we have presented an ecological extension to ~~cGENIE~~ cGEnIE that opens up this area of investigation. ~~EcoGENIE~~ EcoGEnIE is rooted in size-dependent physiological and ecological constraints (Ward et al., 2012). The ecophysiological parameters are relatively well constrained by observations, even in comparison to simpler ecosystem models that are based on much more aggregated functional groups (Anderson, 2005; Litchman et al., 2007). The size-based formulation has the additional benefit of linking directly to functional aspects of the ecosystem, such as food-web structure and particle sinking (Ward and Follows, 2016).

The aim of this paper is to provide a detailed description of the new ecological component. It is clear from Figure 19 that the switch from the parameterised biological pump to the explicit ecological model has led to a deterioration in the overall ability of ~~cGENIE~~ cGEnIE to reproduce the global distributions of important biogeochemical tracers. This is an acceptable outcome, as our goal here is simply to provide a full description of the new model. Given that the original model was calibrated to the observations in question (Ridgwell et al., 2007a), that process will need to be repeated for the new model before any sort of objective comparison can be made. We also note that ~~EcoGENIE~~ EcoGEnIE is still capable of reproducing approximately 90% of the global variability in DIC, more than 70% for phosphate, oxygen and alkalinity, and more than 50% for surface chlorophyll.

Despite a slight overall deterioration in terms of model-observation misfit, the biogeochemical components of the model retain the key features that should be expected. At the same time, the ecological community conforms to expectations in terms of standing stocks and fluxes, both in terms of large-scale spatial distributions, and the seasonal cycles at specific locations (Figures 14 and 17). Overall patterns of community structure and physiological limitation also follow expectations based on observations and theory.

As presented, the model is limited to three limiting resources (light, phosphorus, and iron) and two plankton functional types (phytoplankton and zooplankton). We have written the model equations and code to facilitate the extension of the model to include additional components. In particular, the model capabilities can be extended by enabling silicon and nitrogen limitation, leveraging the silicon and nitrogen cycles already present in BIOGEM (Monteiro et al., 2012). Adding these nutrients will enable the addition of diatoms and diazotrophs, which are both likely to be important factors affecting the strength of the long-term biological pump (Tyrrell, 1999; Armstrong et al., 2002).

7 Code availability

The model code and user instructions can be found at http://www.seao2.info/mycgenie.html.

SVN revision 9982.

Acknowledgements. This work was supported by the European Research Council 'PALEOGENiE' project (ERC-2013-CoG-617313). BAW thanks the Marine Systems Modelling group at the National Oceanography Centre, Southampton. Satellite ocean colour data (Sea-viewing Wide Field-of-view Sensor [SeaWiFS]) were obtained from the National Aeronautics and Space Administration (NASA) Goddard Space Flight Center.

References

Anderson, T. R.: Plankton functional type modelling: Running before we can walk?, Journal of Plankton Research, 27, 1073–1081, 2005.

Archer, D. E. and Johnson, K.: A model of the iron cycle in the ocean, Global Biogeochemical Cycles, 14, 269–279, 2000.

Armstrong, R. A., Lee, C., Hedges, J. I., Honjo, S., and Wakeham, S. G.: A new, mechanistic model for organic carbon fluxes in the ocean based on the quantitative association of POC with ballast materials, Deep-Sea Research II, 49, 219–236, 2002.

Aumont, O., Maier-Reimer, E., Blain, S., and Pondaven, P.: An ecosystem model of the global ocean including Fe, Si, P co-limitations, Global Biogeochemical Cycles, 17, doi:10.1029/2001GB001 745, 2003.

Aumont, O., Ethé, C., Tagliabue, A., Bopp, L., and Gehlen, M.: PISCES-v2: an ocean biogeochemical model for carbon and ecosystem studies, Geoscientific Model Development, 8, 2465–2513, 2015.

Baas-Becking, L. G. M.: Geobiologie of Inleiding Tot de Milieukunde, Van Stockum & Zoon, The Hague, 1934.

Bacastow, R. and Maier-Reimer, E.: Ocean-circulation model of the carbon cycle, Climate Dynamics, 4, 95–125, 1990.

Bec, B., Collos, Y., Vaquer, A., Mouillot, D., and Souchu, P.: Growth rate peaks at intermediate cell size in marine photosynthetic picoeukaryotes, Limnology and Oceanography, 53, 863–867, 2008.

Behrenfeld, M. J. and Falkowski, P. G.: Photosynthetic rates derived from satellite-based chlorophyll concentration, Limnology and Oceanography, 42, 1–20, 1997.

Bruggeman, J. and Kooijman, S. A. L. M.: A biodiversity-inspired approach to aquatic ecosystem modeling, Limnology and Oceanography, 52, 1533–1544, 2007.

Butenschön, M., Clark, J., Aldridge, J. N., Allen, J. I., Artioli, Y., Blackford, J., Bruggeman, J., Cazenave, P., Ciavatta, S., Kay, S., Lessin, G., van Leeuwen, S., van der Molen, J., de Mora, L., Polimene, L., Sailley, S., Stephens, N., , and Torres, R.: ERSEM 15.06: a generic model for marine biogeochemistry and the ecosystem dynamics of the lower trophic levels, Geoscientific Model Development, 9, 1293–1339, 2016.

Cao, L., Eby, M., Ridgwell, A., Caldeira, K., Archer, D., Ishida, A., Joos, F., Matsumoto, K., Mikolajewicz, U., Mouchet, A., Orr, J. C., Plattner, G.-K., Schlitzer, R., Tokos, K., Totterdell, I., Tschumi, T., Yamanaka, Y., and Yool, A.: The role of ocean transport in the uptake of anthropogenic CO_2, Biogeosciences, 6, 375–390, doi:10.5194/bg-6-375-2009, http://www.biogeosciences.net/6/375/2009/, 2009.

Caperon, J.: Growth response of *Isochrysis galbana* to nitrate variation at limiting concentrations, Ecology, 49, 886–872, 1968.

Carr, M.-E., Friedrichs, M. A. M., Schmeltz, M., Aita, M. N., Antoine, D., Arrigo, K. R., Asanuma, I., Aumont, O., Barber, R., Behrenfeld, M., Bidigare, R., Buitenhuis, E. T., Campbell, J., Ciotti, A., Dierssen, H., Dowell, M., Dunne, J., Esaias, W., Gentili, B., Gregg, W., Groom, S., Hoepffner, N., Ishizaka, J., Kameda, T., le Quéré, C., Lohrenz, S., Marra, J., Mélin, F., Moore, K., Morel, A., Reddy, T. E., Ryan, J., Scardi, M., Smyth, T., Turpie, K., Tilstone, G., Waters, K., and Yamanaka, Y.: A comparison of global estimates of marine primary production from ocean color, Deep-Sea Research II, 53, 541–770, 2006.

Claussen, M., Mysak, L., Weaver, A., Crucifix, M., Fichefet, T., Loutre, M.-F., Weber, S., Alcamo, J., Alexeev, V., Berger, A., Calov, R., Ganopolski, A., Goosse, H., Lohmann, G., Lunkeit, F., Mokhov, I., Petoukhov, .,

Stone, P., and Wang, Z.: Earth system models of intermediate complexity: closing the gap in the spectrum of climate system models., Climate Dynamics, 18, 579–586, 2002.

Dierssen, H. M.: Perspectives on empirical approaches for ocean color remote sensing of chlorophyll in a changing climate, Proceedings of the National Academy of Sciences of the United States of America, 107, 17 073–17 078, 2010.

Doney, S., Lindsay, K., Fung, I., and John, J.: Natural variability in a stable, 1000-yr global coupled climate–carbon cycle simulation, Journal of Climate, 19, 3033–3054, 2006.

Droop, M. R.: Vitamin B12 and Marine Ecology, IV. The kinetics of uptake, growth and inhibition in *Monochrysis lutheri*, Journal of the Marine Biological Association of the United Kingdom, 48, 689–733, 1968.

Edwards, N. and Marsh, R.: Uncertainties due to transport-parameter sensitivity in an efficient 3-D ocean-climate model, Climate Dynamics, 24, 415–433, 2005a.

Edwards, N. R. and Marsh, R.: Uncertainties due to transport-parameter sensitivity in an efficient 3-D ocean-climate model, Climate Dynamics, 24, 415–433, 2005b.

Falkowski, P. G., Katz, M. E., Knoll, A. H., Quigg, A., Raven, J. A., Schofield, O., and Taylor, F. J. R.: The Evolution of Modern Eukaryotic Phytoplankton, Science, 305, 354–360, 2004.

Finkel, Z. V., Beardall, J., Flynn, K. J., Quigg, A., Rees, T. A. V., and Raven, J. A.: Phytoplankton in a changing world: cell size and elemental stoichiometry, Journal of Plankton Research, 32, 119–137, 2010.

Flynn, K. J.: The importance of the form of the quota curve and control of non-limiting nutrient transport in phytoplankton models, Journal of Plankton Research, 30, 423–438, 2008.

Follows, M. J., Dutkiewicz, S., Grant, S., and Chisholm, S. W.: Emergent Biogeography of Microbial Communities in a Model Ocean, Science, 315, 1843–1846, 2007.

Friedrichs, M. A. M., Hood, R. R., and Wiggert, J. D.: Ecosystem model complexity versus physical forcing: Quantification of their relative impact with assimilated Arabian Sea data, Deep-Sea Research II, 53, 576–600, 2006.

Friedrichs, M. A. M., Dusenberry, J. A., Anderson, L. A., Armstrong, R., Chai, F., Christian, J. R., Doney, S. C., Dunne, J., Fujii, M., Hood, R. R., McGillicuddy, D., Moore, J. K., Schartau, M., Spitz, Y. H., and Wiggert, J. D.: Assessment of skill and portability in regional marine biogeochemical models: the role of multiple planktonic groups, Journal of Geophysical Research, 112, 2007.

Garcia, H. E., Locarnini, R. A., Boyer, T. P., Antonov, J. I., Zweng, M. M., Baranova, O. K., and Johnson, D. R.: World Ocean Atlas 2009, Volume 4: Nutrients (phosphate, nitrate, and silicate). NOAA Atlas NESDIS 71, U.S. Government Printing Office, Washington, D.C., 2010.

Geider, R. J., MacIntyre, H. L., and Kana, T. M.: A dynamic regulatory model of phytoacclimation to light, nutrients and temperature, Limnology and Oceanography, 43, 679–694, 1998.

Gibbs, S. J., Bown, P. R., Ridgwell, A., Young, J. R., Poulton, A. J., and O'Dea, S. A.: Ocean warming, not acidification, controlled coccolithophore response during past greenhouse climate change., Geology, 44, 59 – 62, doi:10.1130/G37273.1, 2015.

Guidi, L., Stemmann, L., Jackson, G. A., Ibanez, F., Claustre, H., Legendre, L., Picheral, M., and Gorsky, G.: Effects of phytoplankton community on production, size and export of large aggregates: A world-ocean analysis, Limnology and Oceanography, 54, 1951–1963, 2009.

Hain, M. P., Sigman, D. M., and Haug, G. H.: The biological pump in the past, in: Treatise on Geochemistry, vol. 8, pp. 485–517, Elsevier, 2nd edn., 2014.

Hansen, P. J., Bjrnsen, P. K., and Hansen, B. W.: Zooplankton grazing and growth: Scaling with the 2-2,000-μm body size range, Limnology and Oceanography, 42, 678–704, 1997.

Hargreaves, J. C., Annan, J. D., Edwards, N. R., and Marsh, R.: An efficient climate forecasting method using an intermediate complexity Earth System Model and the ensemble Kalman filter, Climate Dynamics, 23, 745–760, doi:10.1007/s00382-004-0471-4, http://dx.doi.org/10.1007/s00382-004-0471-4, 2004.

Heinze, C., Maier-Reimer, E., and Winn, K.: Glacial pCO_2 reduction by the world ocean: Experiments with the Hamburg carbon cycle model, Paleoceanography, 6, 395–430, 1991.

Hollowed, A. B., Barange, M., Beamish, R. J., Brander, K., Cochrane, K., Drinkwater, K., Foreman, M. G. G., Hare, J. A., Holt, J., Ito, S., Kim, S., King, J., Loeng, H., MacKenzie, B. R., Mueter, F. J., Okey, T. A., Peck, M. A., Radchenko, V. I., Rice, J. C., Schirripa, M. J., Yatsu, A., and Yamanaka, Y.: Projected impacts of climate change on marine fish and fisheries, ICES Journal of Marine Science, 5, 1023–1037, 2013.

Hülse, D., Arndta, S., Wilson, J. D., Munhoven, G., and Ridgwell, A.: Understanding the causes and consequences of past marine carbon cycling variability through models, Earth-Sience Reviews, 2017.

John, E., Wilson, J., Pearson, P., and Ridgwell, A.: Temperature-dependent remineralization and carbon cycling in the warm Eocene oceans, Palaeogeography, Palaeoclimatology, Palaeoecology, 413, 158 – 166, doi:http://dx.doi.org/10.1016/j.palaeo.2014.05.019, http://www.sciencedirect.com/science/article/pii/S0031018214002685, selected Papers, Geologic Problem Solving with Microfossils3, 2014.

Kraus, E. B. and Turner, J. S.: A one-dimensional model of the seasonal thermocline II. The general theory and its consequences, Tellus, 19, 98–106, 1967.

Kwiatkowski, L., Yool, A., Allen, J. I., Anderson, T. R., Barciela, R., Buitenhuis, E. T., Butenschön, M., Enright, C., Halloran, P. R., Quéré, C. L., de Mora, L., Racault, M.-F., Sinha, B., Totterdell, I. J., , and Cox, P. M.: iMarNet: an ocean biogeochemistry model intercomparison project within a common physical ocean modelling framework, Biogeosciences, 11, 7291–7304, 2014.

Le Quéré, C.: Reply to Horizons article 'Plankton functional type modelling: running before we can walk?' Anderson (2005): I. Abrupt changes in marine ecosystems?, Journal of Plankton Research, 28, 871–872, 2006.

Le Quéré, C., Harrison, S. P., Prentice, I. C., Buitenhuis, E. T., Aumont, O., Bopp, L., Claustre, H., Cotrim da Cunha, L., Geider, R., Giraud, X., Klaas, C., Kohfeld, K. E., Legendre, L., Manizza, M., Platt, T., Rivkin, R. B., Sathyendranath, S., Uitz, J., Watson, A. J., and Wolf-Gladrow, D.: Ecosystem dynamics based on plankton functional types for global ocean biogeochemistry models, Global Change Biology, 11, 2016–2040, 2005.

Lenton, T. M., Marsh, R., Price, A. R., Lunt, D. J., Aksenov, Y., Annan, J. D., Cooper-Chadwick, T., Cox, S. J., Edwards, N. R., Goswami, S., Hargreaves, J. C., Harris, P. P., Jiao, Z., Livina, V. N., Payne, A. J., Rutt, I. C., Shepherd, J. G., Valdes, P. J., Williams, G., Williamson, M. S., and Yool, A.: Effects of atmospheric dynamics and ocean resolution on bi-stability of the thermohaline circulation examined using the Grid ENabled Integrated Earth system modelling (GENIE) framework, Climate Dynamics, 29, 591–613, 2007.

Litchman, E., Klausmeier, C. A., Schofield, O. M., and Falkowski, P. G.: The role of functional traits and trade-offs in structuring phytoplankton communities: scalling from cellular to ecosystem level, Ecology Letters, 10, 1170–1181, 2007.

Losa, S. N., Vezina, A., Wright, D., Lu, Y., Thompson, K., and Dowd, M.: 3D ecosystem modelling in the North Atlantic: Relative impacts of physical and biological parameterisations, Journal of Marine Systems, 61, 230–245, 2006.

Maier-Reimer, E.: Geochemical cycles in an ocean general circulation model. Preindustrial tracer distributions, Global Biogeochemical Cycles, 7, 645–677, 1993.

Marañón, E., Cermeño, P., López-Sandoval, D. C., Rodríguez-Ramos, T., Sobrino, C., Huete-Ortega, M., Blanco, J. M., and Rodríguez, J.: Unimodal size scaling of phytoplankton growth and the size dependence of nutrient uptake and use, Ecology Letters, 16, 371–379, 2013.

Marchal, O., Stocker, T. F., and Joos, F.: A latitude-depth, circulation-biogeochemical ocean modelfor paleoclimate studies. Development and sensitivities, Tellus, 50B, 290–316, 1998.

Marsh, R., Müller, S. A., Yool, A., and Edwards, N. R.: Incorporation of the C-GOLDSTEIN efficient climate model into the GENIE framework: "eb_go_gs" configurations of GENIE, Geoscientific Model Development, 4, 957–992, doi:10.5194/gmd-4-957-2011, http://www.geosci-model-dev.net/4/957/2011/, 2011.

Martin, J. H., Knauer, G. A., Karl, D. M., and Broenkow, W. W.: Vertex: carbon cycling in the northeast Pacific, Deep-Sea Research, 34, 267–285, 1987.

Meyer, K. M., Kump, L. R., and Ridgwell, A.: Biogeochemical controls on photic-zone euxinia during the end-Permian mass extinction, Geology, 36, 747–750, 2008.

Meyer, K. M., Ridgwell, A., and Payne, J. L.: The influence of the biological pump on ocean chemistry: implications for long-term trends in marine redox chemistry, the global carbon cycle, and marine animal ecosystems, Geobiology, 14, 207–219, doi:10.1111/gbi.12176, http://dx.doi.org/10.1111/gbi.12176, 2016.

Monteiro, F. M., Follows, M. J., and Dutkiewicz, S.: Distribution of diverse nitrogen fixers in the global ocean., Global Biogeochemical Cycles, 24, doi:10.1029/2009GB003 731, 2010.

Monteiro, F. M., Pancost, R. D., Ridgwell, A., and Donnadieu, Y.: Nutrients as the dominant control on the spread of anoxia and euxinia across the Cenomanian-Turonian oceanic anoxic event (OAE2): Model-data comparison, Paleoceanography, 27, n/a–n/a, doi:10.1029/2012PA002351, http://dx.doi.org/10.1029/2012PA002351, pA4209, 2012.

Monteiro, F. M., Bach, L. T., Brownlee, C., Bown, P., Rickaby, R. E. M., Tyrrell, T., Beaufort, L., Dutkiewicz, S., Gibbs, S., Gutowska, M. A., Lee, R., Poulton, A. J., Riebesell, U., Young, J., and Ridgwell, A.: Calcification in marine phytoplankton: Physiological costs and ecological benefits, Science Advances, 2016.

Moore, C. M., Mills, M. M., Arrigo, K. R., Berman-Frank, I., Bopp, L., Boyd, P. W., Galbraith, E. D., Geider, R. J., Guieu, C., Jaccard, S. L., Jickells, T. D., Roche, J. L., Lenton, T. M., Mahowald, N. M., Marañón, E., Marinov, I., Moore, J. K., Nakatsuka, T., Oschlies, A., Saito, M. A., Thingstad, T. F., Tsuda, A., and Ulloa, O.: Processes and patterns of oceanic nutrient limitation, Nature Geoscience, 2013.

Moore, J. K., Doney, S. C., Kleypas, J. A., Glover, D. M., and Fung, I. Y.: An intermediate complexity marine ecosystem model for the global domain, Deep-Sea Research II, 49, 403–462, 2002.

Najjar, R. G., Sarmiento, J. L., and Toggweiler, J. R.: Downward transport and fate of organic matter in the ocean: Simulations with a general circulation model, Global Biogeochemical Cycles, 6, 45–76, 1992.

Najjar, R. G., Jin, X., Louanchi, F., Aumont, O., Caldeira, K., Doney, S. C., Dutay, J. C., Follows, M. J., Gruber, N., Joos, F., Lindsay, K., Maier-Reimer, E., Matear, R. J., Matsumoto, K., Monfray, P., Mouchet, A., Orr, J. C., Plattner, G. K., Sarmiento, J. L., Schlitzer, R., Slater, R. D., Weirig, M. F., Yamanaka, Y., and Yool, A.: Impact of circulation on export production, dissolved organic matter, and dissolved oxygen in the ocean: Results from Phase II of the Ocean Carbon-cycle Model Intercomparison Project (OCMIP-2, Global Biogeochemical Cycles, 21, doi:10.1029/2006GB002 857, 2007.

Norris, R., Kirtland Turner, S., Hull, P., and Ridgwell, A.: Marine ecosystem responses to Cenozoic global change., Science, 341, doi:DOI: 10.1126/science.1240543, 2013.

Oschlies, A.: Model-derived estimates of new production: New results point to lower values, Deep-Sea Research II, 48, 2173–2197, 2001.

Parekh, P., Follows, M. J., Dutkiewicz, S., and Ito, T.: Physical and biological regulation of the soft tissue carbon pump, Paleoceanography, 21, doi:10.1029/2005PA001 258, 2006.

Raven, J. A.: Why are there no picoplanktonic O_2 evolvers with volumes less than 10^{-19} m^3?, Journal of Plankton Research, 16, 565–580, 1994.

Redfield, A. C.: On the proportions of organic derivatives in sea water and their relation to the composition of plankton, vol. James Johnstone Memorial Volume, Liverpool, pp. 176–192, 1934.

Ridgwell, A. and Death, R.: Iron limitation in an efficient model of global carbon cycling and climate, in prep.

Ridgwell, A. and Schmidt, D. N.: Past constraints on the vulnerability of marine calcifiers to massive carbon dioxide release, Nature Geoscience, 3, 196–200, http://dx.doi.org/10.1038/ngeo755, 2010.

Ridgwell, A., Hargreaves, J. C., Edwards, N. R., Annan, J. D., Lenton, T. M., Marsh, R., Yool, A., and Watson, A.: Marine geochemical data assimilation in an efficient Earth System Model of global biogeochemical cycling, Biogeosciences, 4, 87–104, doi:10.5194/bg-4-87-2007, http://www.biogeosciences.net/4/87/2007/, 2007a.

Ridgwell, A., Zondervan, I., Hargreaves, J. C., Bijma, J., and Lenton, T. M.: Assessing the potential long-term increase of oceanic fossil fuel CO2 uptake due to CO2-calcification feedback, Biogeosciences, 4, 481–492, 2007b.

Schartau, M. and Oschlies, A.: Simultaneous data-based optimization of a 1D-ecosystem model at three locations in the North Atlantic: Part I - Method and parameter estimates, Journal of Marine Research, 61, 765–793, 2003a.

Schartau, M. and Oschlies, A.: Simultaneous data-based optimization of a 1D-ecosystem model at three locations in the North Atlantic: Part II - Standing stocks and nitrogen fluxes, Journal of Marine Research, 61, 795–821, 2003b.

Shigsesada, N. and Okubo, A.: Analysis of the self-shading effect on algal vertical distribution in natural waters, Journal of Mathematical Biology, 12, 311–326, 1981.

Tagliabue, A., Mtshali, T., Aumont, O., Bowie, A. R., Klunder, M. B., Roychoudhury, A. N., and Swart, S.: A global compilation of dissolved iron measurements: focus on distributions and processes in the Southern Ocean, Biogeosciences, 9, 233–2349, 2012.

Tagliabue, A., Aumont, O., DeAth, R., Dunne, J. P., Dutkiewicz, S., Galbraith, E., Misumi, K., Moore, J. K., Ridgwell, A., Sherman, E., Stock, C., Vichi, M., Völker, C., and Yool, A.: How well do global ocean bio-

geochemistry models simulate dissolved iron distributions?, Global Biogeochemical Cycles, 30, 149–174, doi:10.1002/2015GB005289, http://dx.doi.org/10.1002/2015GB005289, 2015GB005289, 2016.

Tang, E. P. Y.: The allometry of algal growth rates, Journal of Plankton Research, 17, 1325–1335, 1995.

Tyrrell, T.: The relative influences of nitrogen and phosphorous on oceanic primary production, Nature, 400, 525–531, 1999.

Ward, B. A. and Follows, M. J.: Marine mixotrophy increases trophic transfer efficiency, net community production and carbon export, Proceedings of the National Academy of Sciences of the United States of America, 113, 2958–2963, 2016.

Ward, B. A., Friedrichs, M. A. M., Anderson, T. R., and Oschlies, A.: Parameter optimisation and the problem of underdetermination in marine biogeochemical models, Journal of Marine Systems, 81, 34–43, 2010.

Ward, B. A., Dutkiewicz, S., Jahn, O., and Follows, M. J.: A size structured food-web model for the global ocean, Limnology and Oceanography, 57, 1877–1891, 2012.

Ward, B. A., Martin, A. P., Schartau, M., Follows, M. J., and Anderson, T. R.: When is a biogeochemical model too complex? Objective model reduction for North Atlantic time-series sites, Progress in Oceanography, 116, 49–65, 2013.

Watson, A. J., Bakker, D. C. E., Ridgwell, A. J., Boyd, P. W., and Law, C. S.: Effect of iron supply on Southern Ocean CO_2 uptake and implications for glacial atmospheric CO_2, Nature, 407, 730–733, 2000.

Westberry, T., Behrenfeld, M. J., Siegel, D. A., and Boss, E.: Carbon-based primary productivity modeling with vertically resolved photoacclimation, Global Biogeochemical Cycles, 22, GB2024, 2008.

Wroblewski, J. S., Sarmiento, J. L., and Flierl, G. R.: An ocean basin scale model of plankton dynamics in the North Atlantic. 1. Solutions for the climatological oceanographic conditions in May, Global Biogeochemical Cycles, 2, 199–218, 1988.

Yool, A., Popova, E. E., and Anderson, T. R.: MEDUSA-2.0: an intermediate complexity biogeochemical model of the marine carbon cycle for climate change and ocean acidification studies, Geoscientific Model Development, 6, 1767–1811, 2013.

Zeebe, R. E. and Wolf-Gladrow, D.: CO_2 in seawater, Elsevier Science, 2001.